ABSTRACT

INVESTIGATION OF FORMATION AND APPLICATIONS OF HIGH-SPEED LIQUID PROJECTILES

by

Oleg Petrenko

The work comprises experimental and numerical studies of generation and application of high-speed liquid projectiles. Numerical models were created for a projectile formation by two kinds of launchers, water extruder and water cannon. In the water extruder the kinetic energy of a fast moving piston is transferred to the water load and extrudes the load at a high speed. By contrast in the water cannon the water load itself accumulates the kinetic energy from the expanding combustion gasses. Then, in the course of water motion through the converging nozzle the energy is redistributed between head and tail of the projectile. This enables us to accelerate the front part of the water load to extremely high velocity which may exceed the speed of sound in the water. Inviscid, quasi-stationary model of water flow in the extruder was applied for investigation of the projectile generation in the water extruder. Unsteady 1-D compressible and incompressible models of water flow in the water cannon were applied for the process investigation. Comparison of the result of application of compressible and incompressible models demonstrated that fluid compressibility and subsequently wave processes in the fluid do not contribute for the fluid acceleration. Thus, the acceleration is due to redistribution of the fluid momentum between different parts of a projectile. The numerical study also demonstrated the feasibility to attain the supersonic velocity in the course of acceleration in a converging nozzle. Of course this phenomenon is possible only for unsteady processes.

An experimental technique was developed and applied for online measurement of the projectile head velocity. The acquired experimental data validated the developed numerical technique. Because the attainment the velocity of 1750m/s was shown experimentally, while the sound speed in the water is 1500m/s, the possibility to reach the supersonic velocity in a converging nozzle was demonstrated experimentally.

The constructed numerical model was integrated into the Nelder-Mead simplex search optimization procedure provided by Matlab and used for evaluation of an optimal parameter of a launcher. Particularly, the possibility of the improvement of the nozzle design was shown.

Feasibility of material processing and explosive setups neutralization with high-speed liquid projectiles was studied experimentally using a water extruder and a water cannon. The series of experiments were carried out to evaluate peculiarities of deformation of ductile and brittle materials in the course of high-speed liquid impact. It was shown that while the depth of penetration into a ductile material is monotonously decreasing with increase of stand-off distance, the effect of stand-off distance onto penetration of brittle material has an extremal character. A series of experiments were carried out in order to investigate the demolition of brittle, deformation of ductile and neutralization of explosive material by the use of high-speed liquid projectile. The feasibility of the development of novel impact-based construction, manufacturing and demining technology based on the use of high-speed liquid projectiles was demonstrated.

INVESTIGATION OF FORMATION AND APPLICATIONS OF HIGH-SPEED LIQUID PROJECTILES

by
Oleg Petrenko

A Dissertation
Submitted to the Faculty of
New Jersey Institute of Technology
in Partial Fulfillment of the Requirements for the Degree of
Doctor of Philosophy in Mechanical Engineering

Department of Mechanical Engineering

January 2007

APPROVAL PAGE

INVESTIGATION OF FORMATION AND APPLICATIONS OF HIGH-SPEED LIQUID PROJECTILES

Oleg Petrenko

12/19/06

Dr. Ernest S. Geskin, Dissertation Advisor — Date
Professor of Mechanical Engineering, NJIT

5/24/07

Dr. Denis Blackmore, Committee Member — Date
Professor of Mathematics, NJIT

12/19/06

Dr. Bernard Koplik, Committee Member — Date
Professor of Mechanical Engineering, NJIT

12/19/06

Dr. Pushpendra Singh, Committee Member — Date
Professor of Mechanical Engineering, NJIT

12/19/06

Dr. Rajpal Sodhi, Committee Member — Date
Professor of Mechanical Engineering, NJIT

BIOGRAPHICAL SKETCH

Author: Oleg P. Petrenko

Degree: Doctor of Philosophy

Date: January 2007

Undergraduate and Graduate Education:

- Doctor of Philosophy in Mechanical Engineering,
  New Jersey Institute of Technology, Newark, NJ, 2007

- Master of Science in Applied Physics and Mathematics,
  Moscow Institute of Physics and Technology, Moscow, Russia, 2000

- Bachelor of Science in Applied Physics and Mathematics,
  Moscow Institute of Physics and Technology, Moscow, Russia, 2000

Major: Mechanical Engineering

Presentations and Publications:

Petrenko, O. P., Geskin, E. S., Atanov, G. A., Semko, A. N., Goldenberg, B. (2004). Numerical Modeling of Formation of High-Speed Water Slugs. *Transactions of ASME, Journal of Fluids Engineering*, 126(2).

Geskin E.S., Petrenko O.P., Rusanova O.A., Semko A.N. (2006). Strength Analysis and Optimization of the Barrel of a Powder Water Cannon. *Strength of Material*. Vol. 38, No 2., pp. 206 – 213.

Geskin, E. S., Petrenko, O. P., Rusanova, O. A., Semko, A. N., Bitardse, T. G. (2005). Application of Numerical Techniques for Optimization of the Water Cannon Design. *Proceedings of 2005 WJTA American Water Jet Conference*. Houston, TX.

Petrenko, O. P., Geskin, E. S., Semko, A. N. (Aug. 21-23, 2005) Mechanics of powder hydrocannon for incompressible fluid. *Proceedings of 2005 WJTA American Waterjet Conference*. Houston, TX.

Samardzic, V., Petrenko, O. P., Geskin, E. S., Atanov, G.A., Semko, A.N., Kovaliov A. V. (Aug. 21-23, 2005)
Innovative jetbased material processing technology. *Proceedings of 2005 WJTA American Waterjet Conference*. Houston, TX.

Geskin, E. S, Samardzic, V., Petrenko O. P., Bitardse, T. G., Atanov, G. A., Semko, A. N., Kovaliov, A. V, Rusanova, O. A. (2005)
Feasibility Study of the Solid Freeform Fabrication of Heterogeneous Parts Using the Liquid Impact. *Proceedings of 2005 NSF DMII Grantees Conference*. Scottsdale, Arizona. Grant DMI – 9900247.

Kluz, K., Geskin, E. S., Goldenberg, B., Shishkin, D.V., Petrenko, O. P. (Sept. 2004).
Ice Based Precision Surface Cleaning, *Proceedings of the 2004 WJTA American Waterjet Conference.* Huston, TX.

Geskin, E. S., Goldenberg, B., Petrenko, O. P., V. Samardzic, Atanov, G. A., Semko, A. N. (Jan 2004).
Investigation of Material Fracturing by High-Speed Water Slugs. Presentation at *Annual Meeting of National Science Foundation Division of Design Manufacturing and Innovating Engineering*, Dallas, TX.

Atanov, G. A., Semko, A. N., Petrenko, O. P., Geskin, E. S., Samardzic, V., Goldenberg, B. (Nov. 16-21, 2003). Peculiarities of the Powder Hydrocannon Operation. *Proceedings of IMECE'03: 2003 ASME International Mechanical Engineering Congress & Exposition.* Washington, D.C. IMECE2003-42788

Atanov, G. A., Geskin, E. S., Petrenko, O. P., Semko, A. N. (Sept. 15-21, 2003)
About influence of different factors on water cannon parameters. *Proceedings of XII conference of scientists of Ukraine, Russia, Belarus: Applied problems of Mathematics and Mechanics.* Sevastopol, Ukraine. pp. 134 – 137.

Petrenko, O. P., Geskin, E. S., Atanov, G. A., Semko, A. N., Goldenberg, B. (Aug. 17-19, 2003).
Investigation of High-Speed Water Slugs. *Proceedings of the 2003 Waterjet Technology Conference*. Houston, TX.

Petrenko, O. P., Samardzic, V., Geskin, E. S., Atanov, G. A., Goldenberg, B., Semko A.N., (Aug. 17-19, 2003).
Investigation of high-speed water slugs. *Proceedings of 2003 WJTA American Waterjet Conference,* Houston, Texas. Paper 6-C. - P. 1-13.

Petrenko, O. P., Geskin E. S., Samardzic, V., Golodenberg, B., Atanov, G. A., Semko, A. N., Kovaliov, A. V. (2003).
Numerical and Experimental Investigation of Formation and Application of High Speed Slugs. Presentation at *NSF Grantees conference*. Birmingham, AL.

Geskin, E. S., Goldenberg, B., Petrenko, O. P., V. Samardzic, Atanov, G. A., Semko, A. N., (Jan 2003).
Investigation of Material Fracturing by High-Speed Water Slugs. Presentation at *Annual Meeting of National Science Foundation Division of Design Manufacturing and Innovating Engineering*. Birmingham, AL.

Petrenko, O. P., Samardzic, V., Geskin, E. S., Goldenberg, B., Atanov, G. A., Semko, A. N., (Nov. 2003).
Application of High-Speed Water Slug Technology in Security Tasks. Presentation at *Symposium on homeland security*. New Brunswick, NJ.

Kluz, K., Geskin, E. S., Goldenberg, B., Petrenko, O. P. (Aug. 2003).
Formation and Application of Fine Ice Particles. *Proceedings of the 2003 Waterjet Technology Conference.* Houston, TX.

Podarevskaya, O. V., Petrenko, O. P., Sudavtzova, V. S., Lisnyak, V. V., Stus, N. V. (2002). Crystallization and Thermodynamic Properties of Titanium Stannides, *Journal of Thermal Analysis and Calorimetry*, Vol. 67, pp. 649-657.

Geskin, E. S., Goldenberg, B., Petrenko, O. P., V. Samardzic, Atanov, G. A., Semko, A. N. (Jan. 2002).
Investigation of Material Fracturing by High-Speed Water Slugs. Presentation at *Annual Meeting of National Science Foundation Division of Design Manufacturing and Innovating Engineering*. San Juan, Puerto Rico.

Petrenko, O. P., Geskin, E. S., Atanov, G. A., Goldenberg, B., Semko, A. N. (Nov. 2002). Investigation of Material Deformation by High Speed Water Slugs. *Proceedings of International Mechanical Engineering Congress and Exhibition (IMECE2002)*, New Orleans, LA.

Petrenko, O. P., Geskin, E. S., Atanov, G. A., Semko, A. N., Goldenberg, B. (Nov. 2002). Numerical Modeling of High-Speed Water Slugs. *Proceedings of International Mechanical Engineering Congress and Exhibition (IMECE2002)*, New Orleans, LA.

Petrenko, O. P., Geskin, E. S., Goldenberg, B., Atanov, G. A., Semko, A. N. (Oct. 2002). Investigation of Material Fracturing by High Speed Water Slugs. *Presentation at 16th International* Conference *on Water Jetting*, Aix-en-Provence, France, In *Water Jetting* Ed. P. Lake, Cranfield: BHR Ltd., pp 533-547.

Geskin, E. S., Goldenberg, B., Petrenko, O. P. (2001).
Investigation of Metal Piercing Using High-Speed Water Slugs. *Proceedings of WJTA American Waterjet Conference* (pp. 395-401), Minneapolis, Minnesota.

To my grandparents, family and fiancé

ACKNOWLEDGEMENT

First of all, the author would like to extend a warm thanks to his research advisor, Professor Ernest Geskin for his invaluable advising and guidance, fatherly support and kind encouragement. The author considers himself to be very fortunate to work and study all these years under the guidance of Dr. Geskin.

The author greatly appreciates the help and suggestions from Professors Denis Blackmore, Bernard Koplik, Pushpendra Singh, and Rajpal Sodhi serving as members of the committee.

The author would like to express his sincere gratitude to the collaborating team from Dontetsk National University: Dr. Gennadiy Atanov, Dr. Aleksandr Semko, Dr. Anatoliy Kovaliov. Most of the presented experimental work was done in collaboration with these renown scientists. Numerical modeling was based on their research and done together with them. The author is proud and greatly appreciates to count them among his friends.

Next, the author wants the extend his appreciation to all the helpful colleagues in the Department of Mechanical Engineering, Andriy Titov, Dmitriy Shishkin, Boris Goldenberg, Valeriy Bezmelnitsyn, Konstantin Babets, Veljko Samardzic, Max Roman, Oleksandr Dybenko, Teimuraz Bitadze. The author appreciates the help of Graduate Study and OISF offices staff especially Dr. Kane, Mrs. Gonzales, Mr. Grundy and Mr. Kline.

Finally the author would like to thank everybody who was supportive and helpful during these years, first of all my family and my fiancé Quan Jin for the exceptional support and encouragement.

TABLE OF CONTENTS

Chapter		Page
1	INTRODUCTION	1
	1.1 Objective	1
	1.2 Background Information	1
2	NUMERICAL MODELING OF WATER EXTRUDER OPERATION	12
3	EXPERIMENTAL STUDY OF THE EXTRUDER OPERATION	22
4	EXPERIMENTAL STUDY OF A WATER CANNON	30
	4.1 Equipment	30
	4.2 Demolition Experiments with Water Cannon	38
	4.3 Explosive Setups Neutralization Experiments	42
	4.4 Concluding Remarks	47
5	NUMERICAL MODELING OF WATER CANNON OPERATION	48
	5.1 Objective	48
	5.2 Powder Combustion Modeling	49
	5.3 Projectile Formation Modeling	51
	5.4 Water Cannon Design Optimization	62
	5.4.1 Problem Statement	62
	5.4.1 Nozzle Geometry Optimization	68
	5.5 Concluding Remarks	72
6	INCOMPRESSIBLE MODEL OF WATER CANNON OPERATION	73
	6.1 Definition of the Model	73
	6.2 Estimation of the Fluid Compressibility Effect	78

TABLE OF CONTENTS
(CONTINUED)

Chapter **Page**

6.3 Numerical Study Of Water Cannon Operation 80

6.4 Mechanism of Fluid Acceleration 87

6.5 Concluding Remarks 88

7 CONCLUSION 88

REFERENCES 89

LIST OF FIGURES

Figure		Page
1.1	Schematic of a water extruder	5
1.2	Schematic of a water cannon	6
2.1	Outflow speed V, and pressure P, vs. time at different piston KE levels. Water load is 4.1g.	16
2.2	Outflow speed and pressure as the functions of time. a) Water load 1.4g. b) Water load 4.1g. Graphs 3, 4, 5, 6 represent the corresponding powder load.	17
2.3	Piston speed during extrusion at different exit nozzle diameters: a) d=1.5 mm, b) d=2.0 mm, c) d=2.5 mm. Graphs 0, 1, 2 correspond to water load of 14, 28 and 42 grams. Powder load – level 5.	19
2.4	Maximum extrusion pressure vs. piston-barrel clearance for different water loads. Deformation of the piston and barrel was taken into account.	20
3.1	Experimental water extruder.	22
3.2	Percussive (a) and non-percussive (b) water extruder designs	23
3.3	Drawing of the experimental extruder device for water load 1.4g.	24
3.4	The effect of piston kinetic energy on penetration. a) KEpist= 481 J, V=.94ml, l=27mm, d=6.6mm b) KEpist= 219 J, V=.25ml, l=10mm, d=6.4mm	24
3.5	Lead penetration parameters vs. SOD	25
3.6	The effect of standoff distance on the slug penetration into the concrete	26
3.7	Image of sequential slug development in the air obtained by 2-D PIV. SOD=36mm, slug front velocity =200m/s	27
3.8	Piercing of stainless steel samples with gas and water using level 3 and level 5 powder charges. 1.1&2.1 were impacted by powder gases stream. The thickness of the samples 1.3&2.3 two times more than other samples.	28
3.9	Piercing an irregular opening in a stainless steel plate. Opening diameter is ~3 times larger extruder nozzle diameter.	29
3.10	Water piercing of a large diameter opening in a steel plate. Opening diameter is about 4 times larger nozzle exit diameter.	29

LIST OF FIGURES
(CONTINUED)

Figure		Page
4.1	Schematic of a water cannon	30
4.2	Detailed schematic of the water cannon used in the experiments	31
4.3	Schematic of the device for measuring water slug's head velocity.	33
4.4	Water slug head's front velocimeter setup. IR LEDs and amplified phototransistors from a photo-interrupter are employed in the sensor. The sensor also has two 1.5mm graphite rods installed. The signals from the graphite and phototransistors are fed to a two-channel oscilloscope.	36
4.5	Captions from the high-speed filming. Water load – 230g; Charge – 70g; Velocity of the slug's front – 1600m/s	37
4.6	Destruction of a 26x30x40 cm scale 300-500 concrete block a) set-up of the experiment b) the moment of destruction c) largest piece of the block	38
4.7	Destruction of concrete brand 300-500 plates: a) set up of the experiment, b) result of interaction with the first plate, c) result of interaction with the second plate	39
4.8	Destruction of concrete brand 300-500 block a) set up of the experiment b), c) results of water-concrete interaction	39
4.9	Destruction of concrete brand 300-500 block with a 6 mm steel plate a), b) set up of the experiment c), d) results of the shot	40
4.10	Penetration of three placed together 4.8mm plates with 240g of water using 60g of riffle powder.	41
4.11	Results of two consequent shots to a butt of an armored concrete block with reduced powder charge (30g of powder, 230g of water).	42
4.12	Destruction of an explosive assembly simulation a) set up of the experiment b) water slug scatters the contents of the container c) results of the shot: 5cm hole in the 4mm steel plate, bottom part of the container	44
4.13	Successful neutralization of a soft-case explosive setup.	44
4.14	Experiment on neutralization of a hard-case explosive setup. a), b) The setup and the water cannon installation. c) Explosion of the setup	45

LIST OF FIGURES
(CONTINUED)

Figure **Page**

4.15 Experiment on neutralization of an offensive hand grenade. a) The initial setup b) Moment of explosion c) After the explosion. 46

5.1 Schematic of the mesh 54

5.2 A grid cell schematic 55

5.3 Schematic for equation 5.13 55

5.4 Distribution of water velocity during the process of 200g slug flow in the nozzle. Point of origin is shifted up to the moment of inflow 57

5.5 Outflow velocity vs. time at different barrel lengths 58

5.6 Outflow velocity vs. time at different velocities of the slug inflow in to the nozzle 58

5.7 Outflow velocity vs. time at different water loads. 59

5.8 Slug kinetic energy integral vs. water load at different gunpowder charges. 60

5.9 Outflow velocity vs. time at different gas pressures acting on the slug during its flow in the nozzle. 61

5.10 Integral Effective kinetic energy vs. nozzle diameter at different water loads. 62

5.11 Kinetic energy integrals vs. water loads at different nozzle lengths. 62

5.12 Steepest Descent Method on Rosenbrock's Function (Eq. 1.3). Taken from MATLAB User Manual 65

5.13 Initial a) and optimized b) nozzle profiles 69

5.14 Maximum outflow velocity of a slug at different nozzle configurations. 71

5.15 Effective momentum integral of a slug at different nozzle configurations. 71

5.16 Effective kinetic energy integral of a slug at different nozzle configurations. 71

6.1 Variation of water velocity at the exit of a hydro cannon nozzle for different fluid models. 81

6.2 Outflow velocity for cannon of 3m barrel length. 82

LIST OF FIGURES
(CONTINUED)

Figure		Page
6.3	Outflow velocity of 115g water load, with 700g powder and 2m barrel.	83
6.4	Outflow velocity of 460g water load, with 700g powder and 2m barrel.	83
6.5	Velocity of water outflow from a cannon with long collimator (0.4m)	84
6.6	Velocity of water outflow from a cannon with nozzle exit 0.94 of barrel dia.	84
6.7	Velocity of water outflow from a cannon with nozzle exit 0.34 of barrel dia.	85
6.8	Effect of the powder charge mass on initial outflow velocity	85
6.9	Effect of nozzle diameter on initial outflow velocity	86

NOMENCLATURE

F_c – area of the moving boundary chamber, m^2

J_g – rate of increase of the powder gases mass, kg/s

k – adiabatic constant of powder gases, non-dimensional

L_{nzl} – length of the nozzle

L_{con1} – length of the first of the two cones constituting the nozzle

m_p – powder mass

m_{p0} – initial powder mass, kg

p_g – pressure of powder gases, Pa

p_{gi} – gas pressure after initiator discharge, Pa

q – specific heat of combustion, J/kg

r_{col} – collimator radius

R_{inlet} – inlet radius of the nozzle

R_{outlet} – outlet radius of the nozzle

R_{con1} – radius of the connection between two cones constituting the nozzle

t – time, s

t_{stop} – time of integration (3.1) stop

T – gas temperature

T_o – temperature of powder combustion, K°

u_1 – combustion velocity constant, m/s Pa

u_g – velocity of the combustion chamber boundary movement, m/s

v – specific volume of powder gases, m^3

v – outflow velocity in section 5.4

v_{max} – maximum outflow velocity attained during a shot in section 5.4

V_g – volume, occupied by powder gases, m^3

y – optimization variable, $y=R_{con1}$

x – optimization variable, $x=L_{con1}$

z – ratio of the burned powder layer to the characteristic thickness of the grain, non-dimensional, $z \in [0, 1]$

α – co-volume of powder gases, correction term taking into account molecule volume, m^3

χ_1 – powder grain geometry coefficient pertinent to equation 1e.

h_1 – characteristic thickness of grain, m

λ – powder grain geometry coefficient pertinent to (1e) , non-dimensional

μ – powder grain geometry coefficient pertinent to (1e) , non-dimensional

$\sigma(z)$ – function of z equal to the ratio of grain area at current z and $z=0$

ρ_o – water density at normal conditions

ρ_p – density of the solid powder, kg/m^3

CHAPTER 1

INTRODUCTION

1.1 Objective

High-speed liquid projectiles on impacting an obstacle create high pressures and release kinetic energy at a high rate. The objective of this study is to investigate the feasibility of new material processing technologies based on a high-speed liquid impact, to create tools for studying the formation of high-speed liquid projectiles, to develop techniques for improving existing liquid projectiles launchers.

1.2 Background Information

A high-speed stream of water, referred to as a water jet (WJ) proved to be an efficient tool for mechanical material processing. Its applications range from rock crushing to eye surgery. The WJ is a clean and non-damaging tool that does not contaminate the impact site.

A pure water jet is generated by compressing water to 70-1,000 MPa and subsequently extruding it through a round orifice. The diameter of the orifice ranges from 50 to 350 microns. The water speed at the stagnation pressure of 340 MPa is about 800 m/s. The depth of the WJ penetration is controlled by the water pressure traverse rate, nozzle diameter and standoff distance. Guided by a robotic arm, the WJ generates a desired workpiece surface. A WJ readily penetrates comparatively soft materials, e.g. plastic, fabric, leather, food, etc. Hard materials like granite, high strength steel, etc. are eroded

by the high-speed water stream rather slowly. This shortcoming limits water jet application in material machining.

Inability of the pure WJ to machine hard materials is due to peculiarities of the waterjet-workpiece interaction. Water brought to the substrate surface by a WJ accumulates in the impingement zone. The developed water blanket softens the jet impact and protects substrate material from erosion WJ machining is feasible only if material strength is comparable with the stream stagnation pressure. Pressure increase is a limited solution: with stagnation pressures increased up to 700 MPa the WJ is able to cut thin metal strips, which is not feasible at the conventional stagnation pressure of 300 – 400 MPa.

A more effective way to improve the machining process is to decompose a WJ into a string of droplets. This technology is called a pulse water jet. The material removal by water droplets (pulses) substantially exceeds that of a continuous jet (Conn, 1998, Labus, 1991, Li et al, 1994, Mazurkevich, 1984, Vijay, 1998). In this case water does not accumulate at the impingement zone and incoming droplets impact the unprotected surface of the workpiece. The initial pressure of a droplet impact on a hard surface is equal to ρcv, while stagnation pressure of a continuous jet is $\rho v2/2$. For conventional industrial water jet systems operating at pressures far below 1,250MPa required for obtaining jet flowing with sonic speed, the ratio of the impact pressure to the stagnation pressure, equal to $2c/v$, becomes quite large and the effectiveness of the pulse jet significantly exceeds that of the continuous one.

The impact pressure lasts for a very short time required for a compression wave produced by the impact to travel from the impact site to the jet's free surface and return

back as a rarefaction wave. Material removal by impinging water is enhanced by the stress waves developed in the workpiece during the impact. These waves develop fatigue of the substrate material and subsequent material separation (spallation) This phenomenon determines material erosion by a WJ, even when the material strength exceeds impact stresses. Jet decomposition into droplets significantly increases intensity of the stress waves and, subsequently, material fatigue and spallation.

The practice however, adopted a different approach to the improvement of the jet machining. The conventional WJ was replaced by the Abrasive Water Jet (AWJ), which is a stream of water mixed with abrasive particles. The abrasive particles entrained by the water stream are accelerated almost to the water velocity. The water blanket has no effect on the motion of these particles: they easily penetrate it. Each individual particle, impacting the workpiece surface, forms a dimple. Superposition of the generated dimples results in the material removal. The AWJ is able to machine most of engineering materials. However, the use of particles for momentum transfer from the jet to the workpiece results in the loss of the available energy of the stream. More importantly, a AWJ pollutes the workpiece surface and creates environmental problems. Nevertheless, due to its ability to cut hard-to-machine materials, AWJ are found in a wide range of practical applications.

A water jet possesses a very high concentration of power delivered to the workpiece. This is essential for tasks requiring precise material separation, i.e. cutting. However, in the applications requiring massive material removal, as in mining or in concrete structures demolition, it is the total power delivered, rather than its concentration that plays the major role. Building the high-pressure pumps utilized in water jet is already

a difficult task. Increasing their power to the order of Megawatts is practically an impossible one.

A series of successful experiments in mining and demolition were made with impulsive water jets (IWJ). An IWJ is the material processing technology utilizing discrete ultra-high speed water slugs. Velocities of the slugs can reach several *km/sec.* Impacting a target they effect it similarly to the discharge of a high explosive deposited on the substrate surface, delivering power of 100-700MW. These water slugs can be used for mining and demolition of material of any strength and abrasivity.

The known IWJ devices can be divided into four categories according to the principle of operation accumulators, maximators water extruders and water cannons

Accumulators also employ high-pressure pumps like those used in the stationary WJ. However, water is not directly extruded through a nozzle but gets accumulated in a receiver. After the pressure reaches a certain level a fast-acting valve releases the accumulated energy by letting the water out through a nozzle of a much larger diameter than that used in a conventional waterjet. The produced jet of water has a very high power, many times exceeding the power of the pump (G.G. Yie, 1978, U.H. Mohaupt, et al. 1978). This is the main advantage of accumulators. Tested in construction, they proved to have advantages over conventional tools.

Dynamic pressure of a jet produced by an accumulator is limited by the pump pressure. The main disadvantage of accumulators is a high cost of the high-pressure pump.

Maximators are devices similar to plunger pumps or even more to hydraulic presses. Their main part consists of two rigidly connected pistons with different cross-

sectional areas. A lower supply pressure is acting on the piston with larger cross-section. Consequently, the pressure at the smaller piston is larger than the supply pressure by the factor of the pistons' area ratio. The volume of the water extruded during one cycle is equal to the volume of the high-pressure cylinder. Maximators are also often used for obtaining high stationary pressures for various applications including a stationary waterjet.

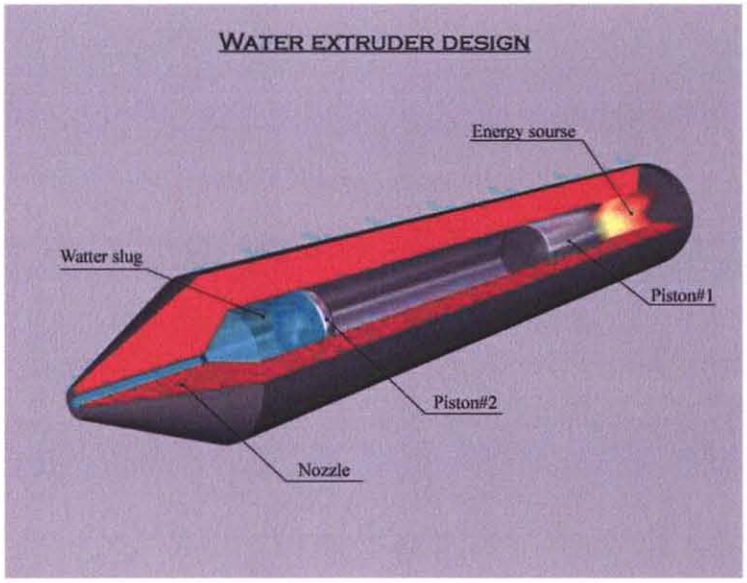

Figure 1.1 Schematic of a water extruder.

Another type of IWJ devices, *water extruders,* is presented in Figure 1.1. They employ a different physical principle of energy accumulation that allows reaching extremely high pressures. The energy is initially accumulated for a short period in the kinetic form in a heavy piston driven by expanding gunpowder combustion gases, compressed air, magnetic field, hydraulic system, etc. The water initially contained at the end of the barrel is impacted by the piston. At impact water is compressed to a high pressure and thus expelled out through a nozzle. Several industrial prototypes for mining and demolition were successfully tested and demonstrated high efficiency (G.P. Chermensky, 1976, G.A. Atanov, 1987, Cooley, W.C., 1972). One of the industrial pilot devices, IV-5,

has a peak pressure up to 1,000 MPa and a firing rate of 20 shots per minute (G.P. Chermensky, 1976). Tested in a coal mine, the extruder demonstrated high potential of being useful in mining. It proved its mining effectiveness as well during tests on rocks with strength of 12 by Protodjakov scale.

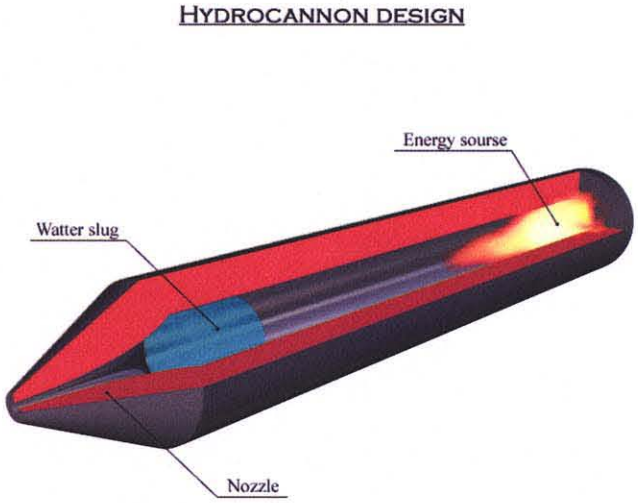

Figure 1.2 Schematic of a water cannon.

Non-stationary undulatory water acceleration to extremely high velocities designates the fourth type of device: *water cannons.* A water cannon consists of a cylindrical barrel with a converging nozzle at the end. The energy source is located at the other end of the barrel. Some water cannon designs can have a metal piston in the barrel. The water load occupies a part of the barrel near the energy source, which could be gunpowder, compressed air, etc. Initially the water load in a form of a cylinder is accelerated in the barrel as a solid projectile would be, with about uniform velocity distribution within the slug. When it enters the converging nozzle complex non-stationary interaction of the water and the nozzle takes place resulting in redistribution of kinetic energy within the slug. The specific kinetic energy of water grows extremely high in a

small front portion of the water load, while it decreases in the rest of the water load. A water cannon enables production of slugs with extremely high velocities. The slug's stagnation pressure of 5,000 MPa is reported to be achieved for water cannon device GA-4 (Patent No. V 2132, E. A. Antonov, 1961, K. P. Stanyukovich, 1955).

There are different variations in the water cannon design. One of the known designs includes a piston between the water and the high-pressure gases. The piston facilitates reducing the water load, providing the equivalent mass of the effective high-speed water slug. Among the disadvantages of this design are wear of the piston, relatively low velocities of the water at the entrance of the nozzle, and the necessity of a hydro-brake preventing the percussion of the piston and the converging nozzle. In other variations the water is located at the entrance of the nozzle. Freely accelerated to high velocities the piston impacts the motionless water load providing it with a velocity almost twice as high as the heavy piston velocity at the moment of percussion G. A. Atanov, 1987).

The nozzle profile doesn't have to be a smooth curve. And what is more, it doesn't have to be continuous. G.A. Atanov has studied a nozzle with a step at the entrance. The step amplifies the initial stage of slug generation. In this work, a systematic search for optimal nozzle profile was attempted (see Section 13 "Nozzle Geometry Optimization").

The water cannon and water extruder were invented and developed at the end of the 1950's in the USSR at the Institute of Hydrodynamics of the Siberian Academy of Science USSR, namely the water cannon GP-4 and several modifications of water

extruders of IV series (E. A. Antonov, 1961, Lavrentjev, M.A., et al., 1961, Lavrentjev, M.A., et al., 1960).

Other IWJ devices, despite the fact that their use is not widespread, should be mentioned.

Electroimpuslive water extruder. This device uses the electrohydraulic effect to expel water from a chamber with a converging nozzle filled with water. A strong electric discharge in the water brings about a quickly growing gas bubble. Its borders proliferate with a velocity of hundreds of meters per second. The pressure rise in the water is undulatory and includes generation of strong shock waves. Thus the average stagnation pressure of the effective slug generated by an electroimpuslive water extruder is significantly smaller than the maximum pressure in the chamber. Due to the absence of moving parts this device, it has some advantages, such as reliability and high rate of multiple projectiles generation.

Elastic barrel water extruder. This device has the design of the water extruder with an elastic impact-proof polymer cylinder filling the high-pressure barrel. There is a coaxial hole in the cylinder filled with water. The speed of sound in the polymer should be higher than in water. Impact of the piston generates a compression wave that travels in the polymer pipe along the nozzle. From the inner surface of the polymer pipe the wave proceeds into the water. As the wave travels along the pipe with speed higher than the sound speed in water, a conic wave is generated in the water load. This conic wave brings about water flow with a radial component towards the barrel axis. Extreme pressure rise in the area of the axis of symmetry results in high-velocity water projectile generation.

A similar conical wave in water is generated using an explosive charge with a cylindrical hole filled with water The detonation wave traveling in the charge along the hole brings about a similar water compression pattern that generates super projectile.

The cumulative effect is known for a long time. Mostly it is known for its use in military applications. The liquid metal projectiles generated by hollow-charge shells reach velocities of several kilometers per second and are capable of penetrating up to 50cm of armor. In engineering elongated shaped charges are used for cutting metal plates. Generation of water slugs using cumulative effect is problematic due to the necessity of the prior formation of a curved free water surface. An innovative device for water projectiles generation is suggested in (Petrenko, E.S., 2002). Here a free surface is formed by placing an air-filled top of a regular plastic bottle in a water reservoir. Detonation of a small explosive charge in the water brings about cumulative effect generating a high-speed water slug. The appeal of the device is its simplicity, low-cost and capability to be constructed in a matter of minutes with improvised means.

In (G.P. Chermensky, 1976) the author discusses industrial water extruder pilot units (IV-5, MPI-2, VIS-1, VBS) created in the Institute of Hydrodynamics SB AS USSR, Dongiprouglemash and Yasinoatskiy engineering plant, VNII-Gidrougol. The water projectiles with the highest stagnation pressure of 1,000 MPa were generated by IV-5 with the rate of 20 shots per minute. Tests of these units in coalmines demonstrated the high effectiveness of water extruders. Problems of wear and durability are shown to be the main issues for water extruders.

B. E. Edney at the Institute CERAC S. A., Switzerland has experimentally studied water slugs with velocities up to 3,500 m/s (B.E. Edney, 1976). The slugs velocity and

their propagation in the air were determined using a $1 \cdot 10^{6}$ fps camera with $20 \cdot 10^{-9}$ s flashes. Four different nozzle profiles were tested both in the air and a vacuum. The experimental results were compared to analytical solutions based on the incompressible flow theory of Ryhming. At velocities above 1,500 m/s the theory was found to be in conflict with the experiment.

I.M. Daniel at IIT Research Institute has conducted an experimental study of 900m/s – 2,800 m/s water slugs using dynamic photoelasticity, embedded strain gages and high-speed photography. Stagnation pressure dynamics was measured by a piezoelectric transducer. Also cratering experiments were conducted with different brittle materials. Statistical correlations of crater volume with jet parameters were produced. (I.M. Daniel, 1976)

The study of A.J. Watson, F.T. Williams and R.G. Brade, University of Sheffield, England investigates propagation of water cannon-produced projectiles in air, and their interaction with targets and pressure measurements at the target impact. Gelled water was accelerated by a powder propellant and photographed using cine photography and X-ray radiography. Strain gages placed on an array of Hopkinson bars were used to measure the pressure exerted by the slug at target impact (Watson, A.J., et al. 1984).

Most of the studies were dedicated to the experimental investigation of water slugs and devices for their generation. Theoretical developments in this area were limited. The constructed models were not suitable for modeling involved processes due to extreme pressures resulting in significant water compressibility, and the high speed of the processes and their undulatory nature, not allowing the consideration of the problems using stationary assumptions. Fundamental work of G.A. Atanov involved numerical and

experimental studies of water cannon and water extruder water slug generation. Numerical models based on the Godunov method and the method of characteristics were developed. Results of these experiments demonstrated the validity of the models over the whole range of experimental parameters with high accuracy.

CHAPTER 2

NUMERICAL MODELING OF THE OPERATION OF WATER EXTRUDER

A sequence of rather complicated phenomena occurs in the course of water extrusion by an impacting piston. These phenomena involve motion of the piston prior to and after the impact, formation and development of compression and rarefaction waves in the fluid, and their interaction with the piston, the walls and each other that results in the fluid flow, energy dissipation, deformation of the piston and the barrel resulting in a piston-barrel clearance that yields water backflow. Preliminary analysis allows identifying which of these phenomena play key a role in the water extrusion process and which could be disregarded.

Large Reynolds numbers of $Re=10^4$ for an industrial scale extruder like IV-5 and of $Re=10^3$ for experimental laboratory setup imply that viscosity can be disregarded with little loss of accuracy.

Water compressibility, on the other hand, should be taken into account due to high pressures developed in extruders and primarily due to nonstationarity of water impact by a piston. At pressures of 1GPa often attained in extruders, water volume reduces by 10%. Computation results for compressible and incompressible fluids differ qualitatively (G.A. Atanov, 1987) at even earlier stages of the extrusion, when fluid pressure is relatively low. The extrusion process starts with a piston impacting water. For incompressible flow idealization water velocity instantaneously should change from zero to a finite value. Such an idealization would be valid if the studied water flow would be far past the initial moment of impact. However with a duration of the whole extrusion process a fraction of millisecond, water compressibility should be taken into account.

Compression waves generated by the piston impact reflect from the extruder walls, piston and the free surface, and interact with themselves. Superposition of the waves eventually results in the water outflow. Modeling of these complex processes could be significantly simplified by assuming the process to be quasi-stationary. In this approach we disregard wave motion and assume uniform parameters distribution in the volume occupied by water. In the experimental device duration of the water flow is about 0.5ms while the compression wave covers the distance between the piston and the nozzle in about 0.01ms. Outflow duration by far exceeds relaxation time of wave processes, so it may be disregarded.

In contrast, heat transfer in the slug can be disregarded because its thermal relaxation time is comparatively long, thus the water extrusion can be considered to be adiabatic. In quasi-stationary approximation it becomes isentropic.

The isentropic equation of Teta provides good approximation for water pressures up to 3 GPa (G.A. Atanov, 1987):

$$\frac{p+B}{\rho^n} = const$$

With these assumptions the internal ballistics of a non-deforming water extruder can be described by a system of ordinary differential equations consisting of an isentropic equation, Bernoulli equation and equations governing the motion of a rigid piston subjected to the pressure of the combustion gases on one side and the water on the other. This model written in the following equations was developed and studied first by G.A. Atanov (G.A. Atanov, 1987):

$$\begin{cases} \dfrac{dp}{dt} = n(p+B)\left(\dfrac{1}{m}\dfrac{dm}{dt} + \dfrac{1}{l_1 - x}\dfrac{dx}{dt}\right) \\ \dfrac{dm}{dt} = -F_a \rho_n c_n \sqrt{\dfrac{2}{n-1}\left[\left(\dfrac{p+B}{B}\right)^{\frac{n-1}{n}} - 1\right]} \\ \dfrac{dw}{dt} = \dfrac{1}{m_1}\left(1 + \dfrac{m_1}{m_2}\right)\left(F_2 p_g - F_1 p\right) \\ \dfrac{dx}{dt} = w \end{cases} \tag{2.1}$$

Here the first equation is the Teta equation of isentropic water compression in differential form ($n=k=C_p/C_v= 7.15$), the second is the Saint-Venant formula which is equivalent to the Bernoulli equation with stagnation parameters inside of the extruder and zero pressure on the nozzle exit, the third and fourth equations are the Newton laws, governing the motion of the piston of mass m_1 inside of a free extruder of mass m_2.

These equations describe water extrusion with a rigid non-deforming device. High pressure inside the barrel (up to 1GPa) leads to its deformation and changes its inner volume. With a large adiabatic coefficient for water ($n=7.15$) even a small volume variation results in a significant pressure change. Thus, it is necessary to take into account the change of the barrel radius and the piston length as well.

The deforming barrel can be approximated by an infinitely long cylinder with thick walls. Then its deformation can be determined by the Lame equation:

$$\Delta R_{inn} = p\frac{R_{inn}}{E}\left(\frac{R_{out}^2 + R_{inn}^2}{R_{out}^2 - R_{inn}^2} + \mu\right) \tag{2.2}$$

For steel $E \approx 2.05 \cdot 10^{11}$ Pa and $\mu \approx 0.3$;

Piston deformation is defined accordingly as

$$\Delta l_p = l_p \frac{\sigma}{E} \tag{2.3}$$

$$\sigma = p + \frac{m'}{2F_1}\frac{dw}{dt} \tag{2.4}$$

This leads to the suggestion by G.A. Atanov, modified for a deformation system of equations describing the internal ballistics of a water extruder [1,2]:

$$\begin{cases} \dfrac{dp}{dt} = \dfrac{\dfrac{1}{m}\dfrac{dm}{dt} + \dfrac{1}{l_1 - x}\dfrac{dx}{dt}}{\dfrac{1}{n(p+B)} + \dfrac{2}{E}\left(\dfrac{z^2+1}{z^2-1} + \mu\right)} \\ \dfrac{dm}{dt} = -F_a \rho_n c_n \sqrt{\dfrac{2}{n-1}\left[\left(\dfrac{p+B}{B}\right)^{\frac{n-1}{n}} - 1\right]} \\ \dfrac{dx}{dt} = \dfrac{w\left[\dfrac{1}{n(p+B)} + \dfrac{2}{E}\left(\dfrac{z^2+1}{z^2-1} + \mu\right)\right] - \dfrac{l_p}{Em_1}\left(1 - \dfrac{m'}{2m_1}\right)\dfrac{dm}{dt}}{\dfrac{1}{n(p+B)} + \dfrac{2}{E}\left(\dfrac{z^2+1}{z^2-1} + \mu\right) - \dfrac{l_p}{E(l_1 - x)}\left(1 - \dfrac{m'}{2m_1}\right)} \\ \dfrac{dw}{dt} = \dfrac{1}{m_1}\left(1 + \dfrac{m_1}{m_2}\right)\left(F_2 p_g - F_1 p\right) \end{cases} \tag{2.5}$$

Numerical studies of the simplified and adjusted systems has shown that elastic deformations in the device reduce the maximum pressure by 10 – 15% (G.A. Atanov, 1987).

The other effect significantly weakening extruder performance is the flow between the sealing piston and the barrel. With this channel additional to the nozzle opening the maximal water pressure in the barrel reduces. As a result, maximal water outflow velocity reduces as well. This effect can be taken into account by assigning F_a – rather then just the nozzle exit area – the combined effective area (G.A. Atanov, 1987), which is the sum of the nozzle exit area and the clearance area multiplied by the friction losses coefficient $\varphi_c \approx 0.9$: $F_a = F_{nozzle} + \varphi_c \cdot F_{clearance}$. However the clearance size is not

constant; it changes as the piston and the barrel deform under high pressure. Even though this deformation is small, the clearance size initially is also very small, within machining tolerances, and thus varies significantly. Thus, F_a in the equations (2.5) should be a function of the/a pressure $F_a(p)$ rather than a constant.

A typical example of numerical integration of the system (5) is shown in Figure 2.1. Pressure in the barrel p and water outflow speed v depicted there are the main parameters of interest. The calculations were carried out for the extruder parameters, water load and powder charge corresponding to the carried out experiments. Water behavior in the course of the slug formation and acceleration explains the form of the generated curves.

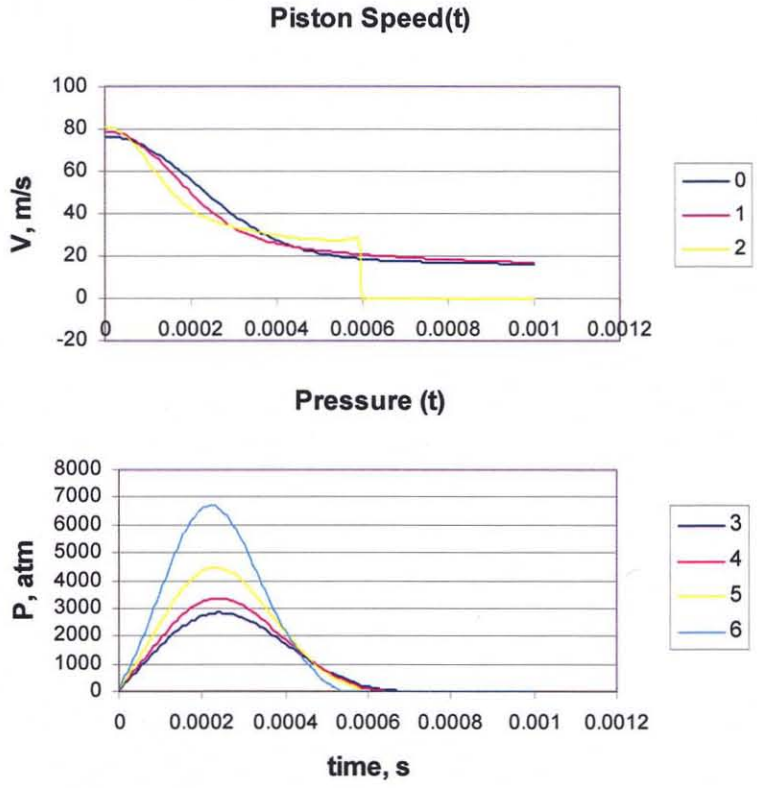

Figure 2.1 Outflow speed V, and pressure P, vs. time at different piston KE levels. Water load is 4.1g.

According to the quasi-stationary assumption at the moment of impact pressure in the barrel and outflow velocity is still zero. As the piston moves forward, it compresses water in the barrel increasing its pressure and, consequently, outflow velocity. In this interaction the piston performs work on the water load spending its own kinetic energy acquired form the powder combustion gases in the preceding acceleration stage. As a result, the piston's kinetic energy is converted into the internal (compression) and kinetic (acceleration) energies of the water. At some moment, piston deceleration and accordingly water pressure and outflow velocity reach a maximum. Then $v_{outflow\ max}=V_{piston}\cdot F_{barrel}/F_a$. Further piston deceleration is accompanied with pressure reduction.

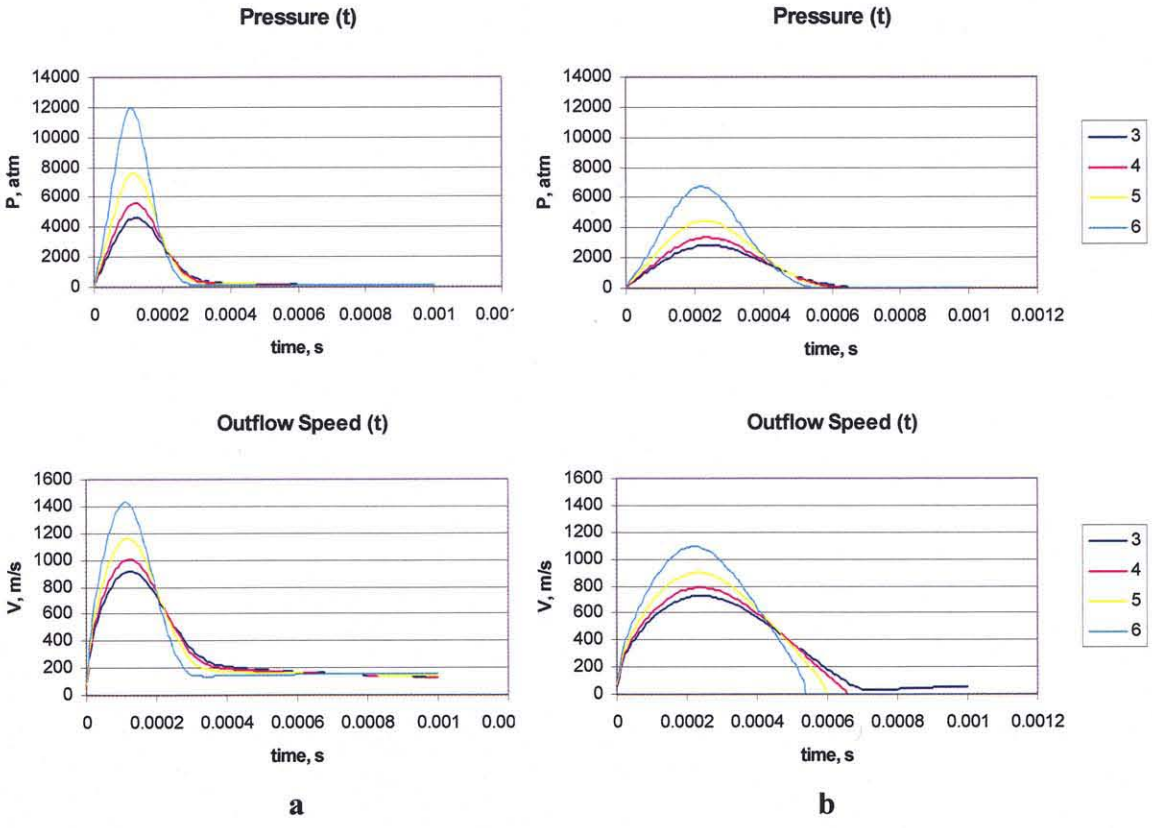

Figure 2.2 Outflow speed and pressure as functions of time
a) Water load 1.4g
b) Water load 4.1g
Graphs 3, 4, 5, 6 represent the corresponding powder load.

The numerical calculations enabled us to evaluate the change of the process variables (pressure in the barrel, exit velocity of the slug). Figure 2.2 depicts the change of the water pressure and exit water velocity at water masses of 1.4 g and 4.1 g and at various powder charges. The kinetic energy of the piston in these experiments ranged from 191 J to 515 J corresponding to the standard Remington powder charge levels from 3 to 6. As it follows from these charts, reduction of the water mass increases the maximal value of the slug velocity that is the maximal impact force, while it also decreases the outflow duration. Thus, the charts in the Figure 2.2 provide guidance to the selection of the extruder load that optimizes the results of the slug-target interaction. Of course the knowledge of conditions of the target fracturing is required for such a selection.

Numerical solution of the system (2.1) and (2.5) provides understanding of the extruder parameters influence on the produced water slug and provides means for design of the experimental extruder set up (Figure 1.1), which constituted a modified Remington power tool. The set up could operate on three levels of water load (1.4, 2.8 and 4.1 grams) and on five standard powder charges of levels 2 (0.111g), 3 (0.144g), 4 (0.177g), 5 (0.244g) and 6 (0.389g). The powder energy in parted to the piston (105 g) ranged from 137 to 539 J.

When designing an extruder device it is preferable to achieve near full utilization of the piston kinetic energy. It is attained when the piston stops at the end of extrusion process without bouncing back or impacting the nozzle. While piston rebound is undesirable, its impact at the nozzle is unacceptable – it will cause damage to the device if not by breaking of the piston then by its deformation and jamming of the device. The Figure 2.3 shows piston velocity charts presenting a set of calculations done for a

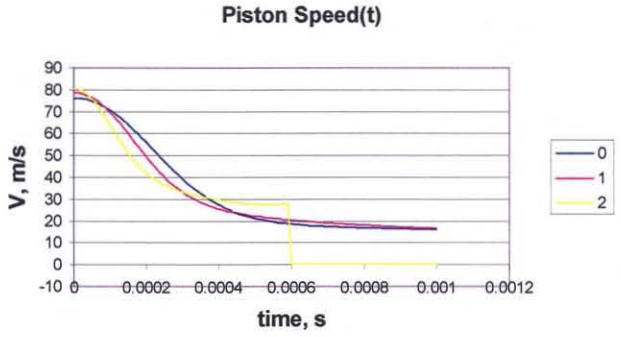

b

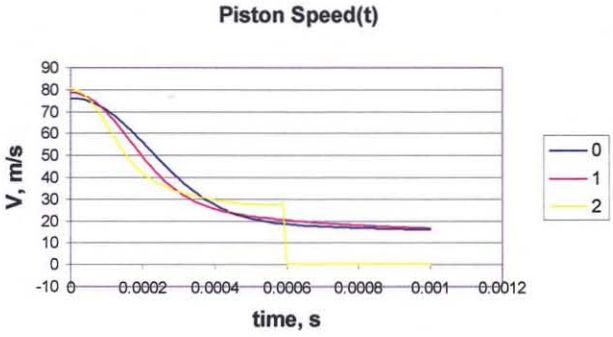

a

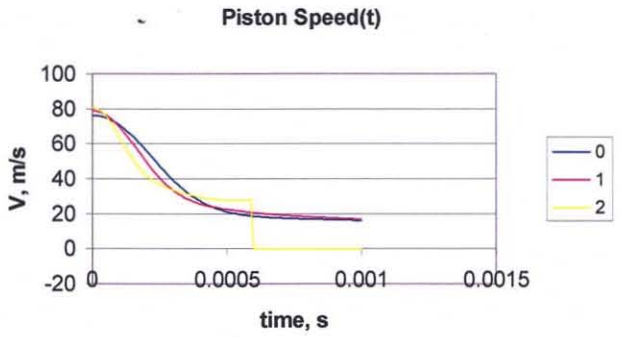

c

Figure 2.3 Piston speed during extrusion at different exit nozzle diameters
a) d=1.5 mm
b) d=2.0 mm
c) d=2.5 mm

Graphs 0, 1, 2 correspond to water load of 14, 28 and 42 grams. Powder load – level 5

selection of nozzle diameters. Small nozzle diameter results in higher maximal pressure but in partial utilization of the piston kinetic energy, because the piston bounces back at a relatively high velocity. A rather large nozzle diameter produces small pressure and thus small outflow velocity, doesn't fully utilize piston kinetic energy and what's most important results in the piston impacting the nozzle with high speed. Near optimum nozzle diameter provides either light piston impact or small rebound assuring device durability and near complete utilization of piston KE.

The objective of another series of computations was to evaluate the effect of machining quality and barrel wear on the extruder performance. More specifically, the effects of the water flow in the piston-barrel clearance as well as the effect of the deformation of the barrel and the piston on the maximum pressure attained in the barrel

were determined. Here the deformation of the barrel and the piston were also taken into account.

The estimated effect of the clearance on the maximum pressure attained in the course of extrusion is depicted on the Figure 2.4. As it follows from the chart this effect depends on the water load. The maximum water pressure and thus the maximum outflow speed are influenced mostly by the gap size at the minimal water load. The clearance of 0.002", which is a standard machining tolerance, results in more than 30% drop of the maximum extrusion pressure (Figure 2.4)

The effect of the deformation was estimated at the ratio of outer to the inner barrel diameters close to 4. As it follows from performed computations even at this, a rather favorable ratio extruder deformation reduces the maximal available water pressure up to 10%.

Deformation of the barrel, subjected to the static water pressure, increases the opening between the barrel and the piston during the water extrusion. This intensifies the

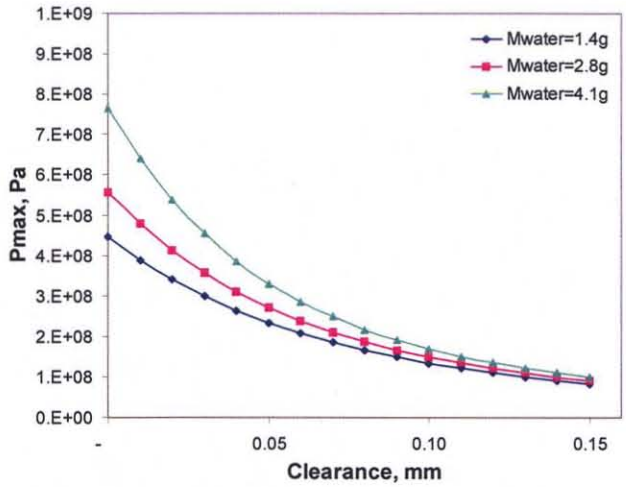

Figure 2.4 Maximum extrusion pressure vs. piston-barrel clearance for different water loads. Deformation of the piston and barrel was taken into account.

effect of the clearance flow and thus degrades the extruder's performance even more.

The piston-barrel gap cannot be controlled. As the piston wears out, the gap increases. This gap growth as well as the metal deformation predictably reduces the effectiveness of the extruder. In the actual devices the negative effect of the piston-barrel clearance flow can be addressed by self-packing seals and seals deforming under pressure to compensate barrel-piston clearance increase.

CHAPTER 3

EXPERIMENTAL STUDY OF THE EXTRUDER OPERATION

While the internal ballistics of the extruder is well understood and documented, the slug behavior in the course of the motion outside the nozzle (external ballistics) and especially the slug interaction with a target are not predictable and nor well understood. In order to address this issue in the presented study, a series of experiments were conducted to investigate water slug-target interaction. Better understanding of this process is necessary for setting criteria on the water slug properties that would yield the best operating efficiency.

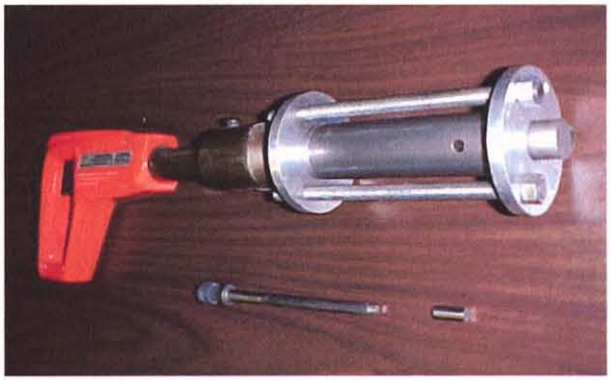

Figure 3.1 Experimental water extruder.

The water extruders used in the performed experiments were built on the base of a Remington power tool. Using the results of the performed calculations, device parameters were selected to maximize utilization of the piston kinetic energy. At the selected conditions the rebounding of the piston and piston impact at the entrance of the nozzle were minimal. Also, the masses of piston and water load were reduced in order to increase the maximum water pressure attained in the course of impact. However in this case the tolerance of the barrel and piston machining became critical. As it was shown

(Figure 2.4) at low water loads even a small gap between the barrel and the piston causes significant pressure reduction. Powder charge and the water load mass could be varied in the setup. The experiments were carried out with the water loads of 1.4 g, 2.8 g and 4.1g and at the powder charges of 0.111g, 0.144g, 0.177g, 0.244g and 0.389g. The piston mass was 105g and the power energy imparted to the piston ranged from 137J to 539J depending on the charge.

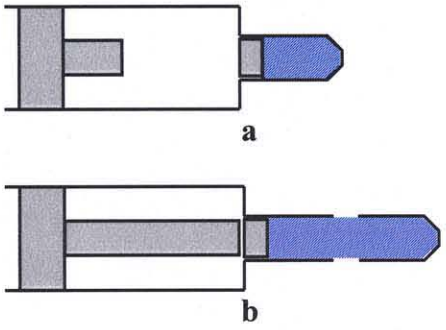

Figure 3.2 Percussive (a) and non-percussive (b) water extruder designs.

Initially the design shown in Figure 3.2a was used for construction of the extruder. Here a heavy piston accelerated by the gunpowder combustion products strikes the smaller piston, sealing the water in the barrel. At this instance the extrusion begins. This design, however, appeared to be unreliable. After a few cycles both pistons were either deformed, if made of a ductile steel, or broken, if made of a hard more brittle steel, making further operation of the device impossible.

In order to eliminate this problem the design shown on the Figure 3.2b was used. In this design a long piston drives the water contained in a long barrel. There are large drainage openings on the barrel walls with the sum of the areas equal to the barrel cross-sectional area. Water escapes through the large drainage openings under negligible water pressure allowing the piston to freely accelerate until the sealing piston passes these

openings and closes them. At this point the water extrusion process begins with the mode of extrusion similar to that in the case a. However in the case of 4b the impact between the two pistons was eliminated. The main advantage of this version is non-percussive operation, which assures device durability. The device 4b was used in further experimental studies of water slug-target interaction. A detailed drawing of the extruder is shown in Figure 3.3.

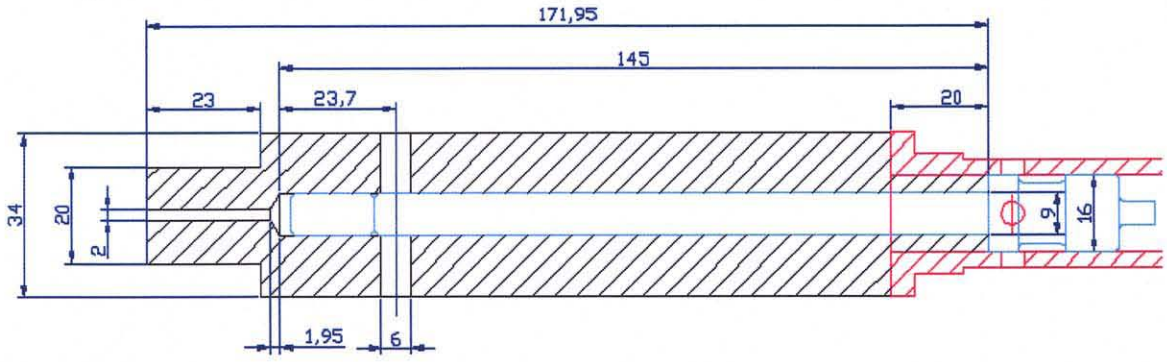

Figure 3.3 Drawing of the experimental extruder device for water load 1.4g.

Two sets of experiments were carried out in order to investigate the target deformation by the impacting slug (Figures 3.4 and 3.6). The behavior of plastic (lead) and brittle materials (concrete) was studied. Predictably they significantly differed. The shape of the cavities generated at the lead surface in the course of an impact was rather

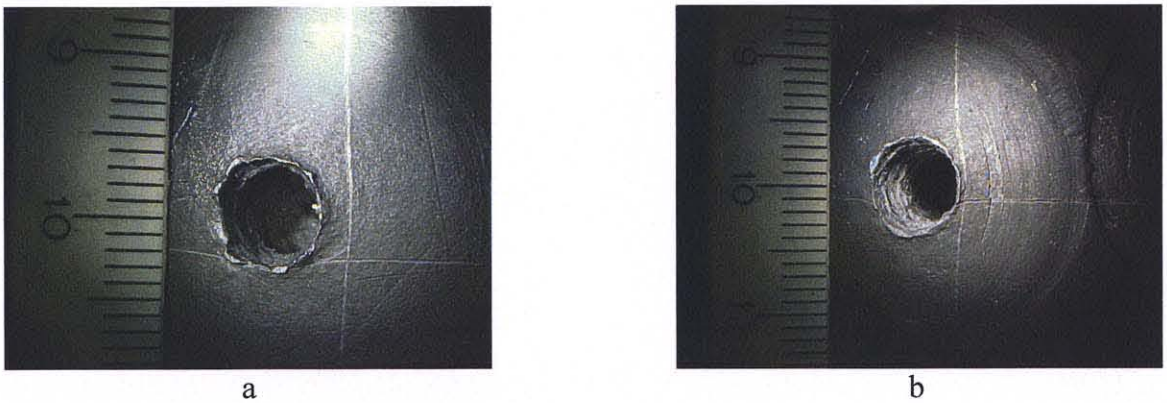

a b

Figure 3.4 The effect of piston kinetic energy on penetration:
a) KE_{pist}= 481 J, V=.94ml, l=27mm, d=6.6mm,
b) KE_{pist}= 219 J, V=.25ml, l=10mm, d=6.4mm.

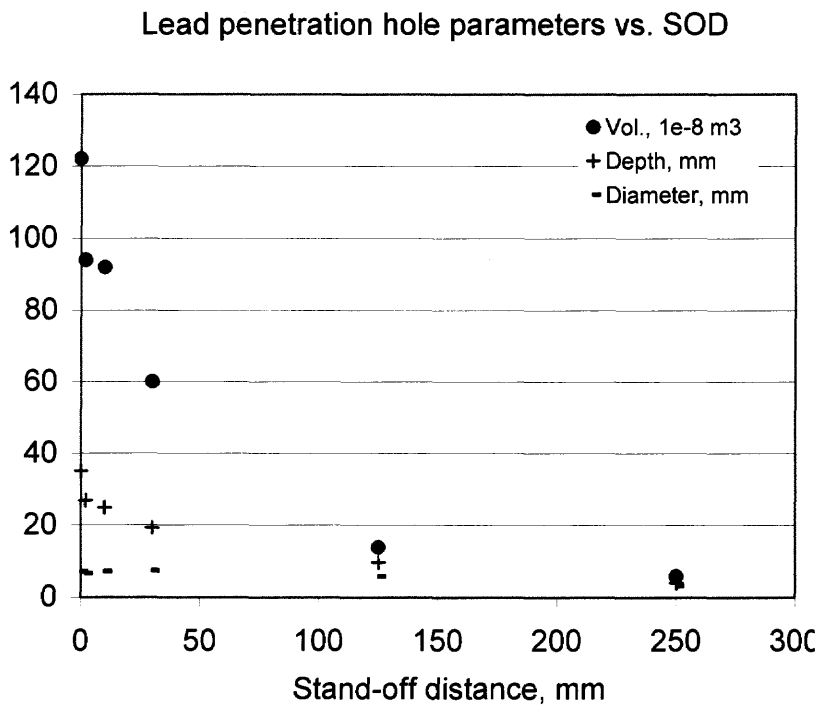

Figure 3.5 Lead penetration parameters vs. SOD.

reproducible. Effects of the standoff distance and the slug's energy at the impact zone on the depth of the penetration (Figure 3.5) appeared to be stable and monotone.

In contrast, the effect of the standoff distance on the concrete fracturing is clearly extremal (Figure 3.6). Contrary to the penetration into lead, where the best results were achieved at zero standoff distance, in the case of the brittle material the maximal penetration is attained at a non-zero standoff distance between the extruder exit and target.

At different standoff distances a target is subject to different impact conditions even if the extrusion processes are identical. This difference is due to the transformation of a slug during its flight. Two main factors play a role in this transformation. One is the destruction of the slug due to interaction with air. The other is the change of the slug structure and velocity distribution due to variation of the outflow velocity. As the outflow

velocity grows in the course of extrusion (Figure 2.1) the faster parts of the slug impact slower parts extruded earlier. This collapsing interaction in the stream generates a radial flow, changes thickness of the slug and, what's crucial for a brittle target, results in the increase of the slug's front velocity.

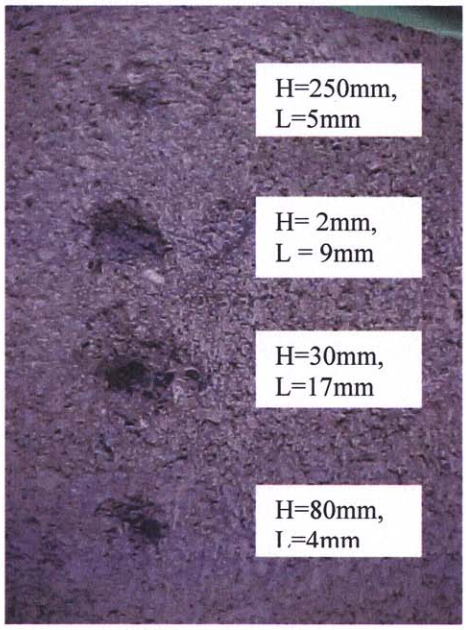

Figure 3.6 The effect of standoff distance on the slug penetration into the concrete.

The increase of the slug's front velocity was registered in experiments performed by the waterjet laboratory staff (Figure 3.7). The velocity was measured with a particle image velocimetry (PIV) technique.

The photograph (Figure 3.7) clearly shows non-uniform water distribution along the slug. There is a clearly seen mushroom-shaped head formed due to interaction with air and due to collapse of slower slug parts with faster parts, extruded afterwards. Also there is a less pronounced bulge in the middle of the jet. The author attributes this to the same collapsing.

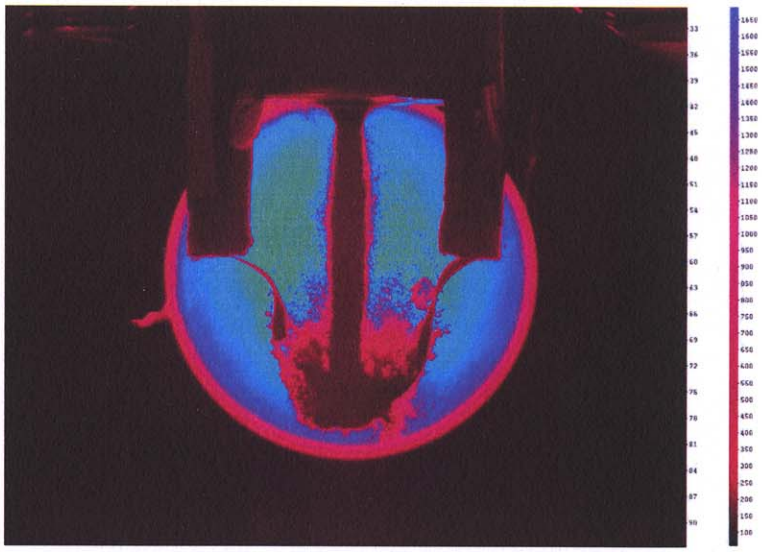

Figure 3.7 Image of sequential slug development in the air obtained by 2-D PIV. SOD=36mm, slug front velocity =200m/s.

At the instant of impact, a pressure of impact equal to ρvc is exerted on the target. Its duration is very short, but at subsonic velocities it is much higher than the dynamic pressure of the slug's stream equal to $\rho v^2/2$.

Brittle materials are characterized by relatively low energy failure but a sufficiently high stress failure. They are characterized by catastrophic destruction as the applied pressure exceeds the strength of the material. Thus the maximum force rather than the apportioned energy determines their failure. The maximum velocity of the slug head is attained in the course of slug development at some optimal standoff distance. This maximum velocity brings about maximum pressure, which exceeds the strength of the concrete.

Penetration of plastic materials has different factors prevailing. Instead of crack formation, as in a brittle material, ductile materials undergo plastic deformation The energy of the impact is comparatively low, so the impact plays a negligible role in the penetration. The further away from the nozzle exit, the more destructed the slug becomes

due to collapsing and interaction with air. So the minimal standoff distance brings about the best penetration results for a ductile material.

Another set of experiments on piercing of aluminum and steel plates has been performed at the minimal stand-off distance. The principal finding of these experiments was a demonstration of the feasibility of metal piercing and deformation using our setup. It was noticed that at similar conditions the explosion products brought about a slight deformation of the substrate. Thus, the use of a slug as a momentum transfer media is necessary.

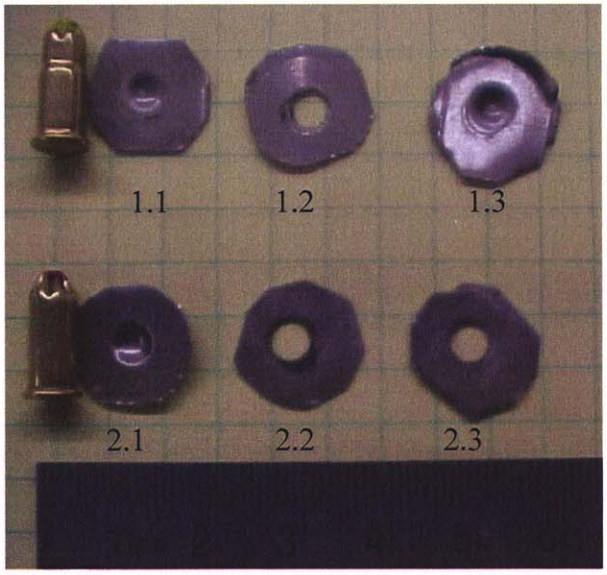

Figure 3.8 Piercing of stainless steel samples with gas and water using level 3 and level 5 powder charges. 1.1&2.1 were impacted by powder gases stream.
The thickness of the samples 1.3&2.3 two times more than other samples.

Figure 3.9 Piercing an irregular opening in a stainless steel plate. Opening diameter is ~3 times larger extruder nozzle diameter.

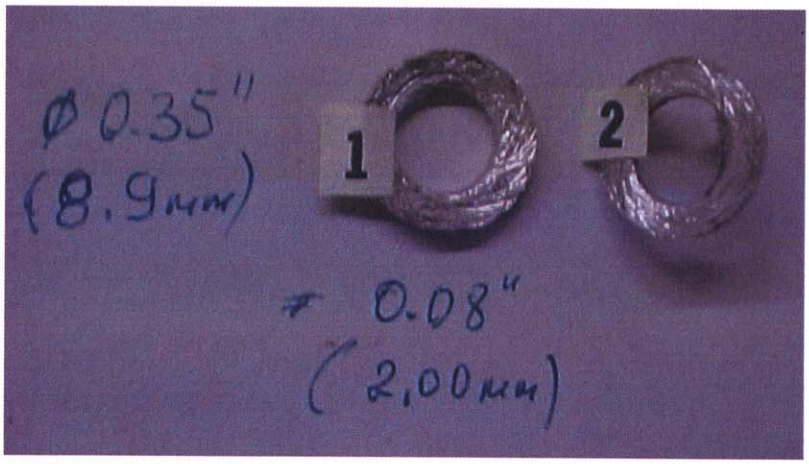

Figure 3.10 Water piercing of a large diameter opening in a steel plate. Opening diameter is about 4 times larger nozzle exit diameter.

/

CHAPTER 4

EXPERIMENTAL STUDY OF A WATER CANNON

4.1 Equipment

Experiments with a small-scale water extruder described in the previous chapter have demonstrated the feasibility of high-speed water slugs to pierce, stamp and penetrate metal, and demolish brittle materials. These basic operations constitute a foundation of a new material processing technology, which utilizes a high-speed liquid impact as the toolpiece.

Productivity of a liquid impact increases with the scale of the impact – diameter of a water slug, its mass and velocity. Employing a larger device and studying capabilities of larger and faster water slugs is the next step in the development of an industrial prototype.

However even small-scale extruder devices posed difficulties in operation, because wear and deformation of the polished and close-fit barrel and the sealing piston cause deterioration of the extruder's performance with time. Large scale water extruders

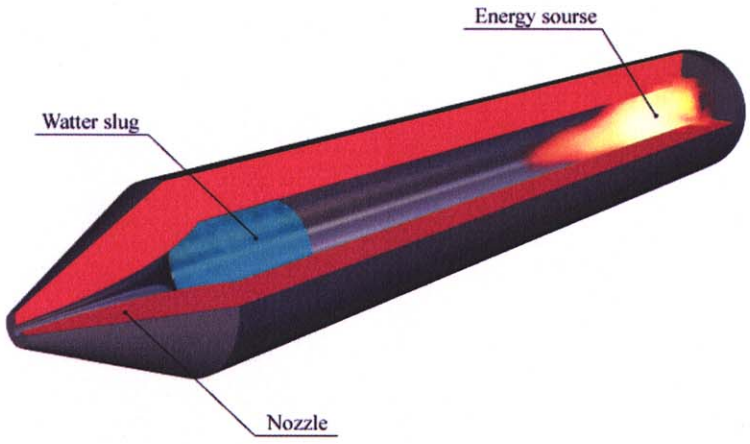

Figure 4.1 Schematic of a water cannon.

tested in the mining industry are more complex in design and require regular maintenance and regular replacement of the worn parts .

A non-percussive watercannon powered by gunpowder (Figure 4.1) is simpler in design and operation. It has no moving parts and the requirements for the surface quality are much lower than for the extruder's barrel and piston walls. This makes the water cannon more reliable and more durable. Another advantage is its capability to generate ultra high-speed water slugs with static pressure inside the barrel much lower than the stagnation pressure of the slug (Atanov, 1987).

For the experimental study of high-speed water slugs and development of IWJ material processing technology, two identical industrial-scale water cannon units were manufactured in Donetsk National University, Ukraine for the Waterjet Laboratory, NJIT. The schematic of the devices is depicted in the Figure 4.2.

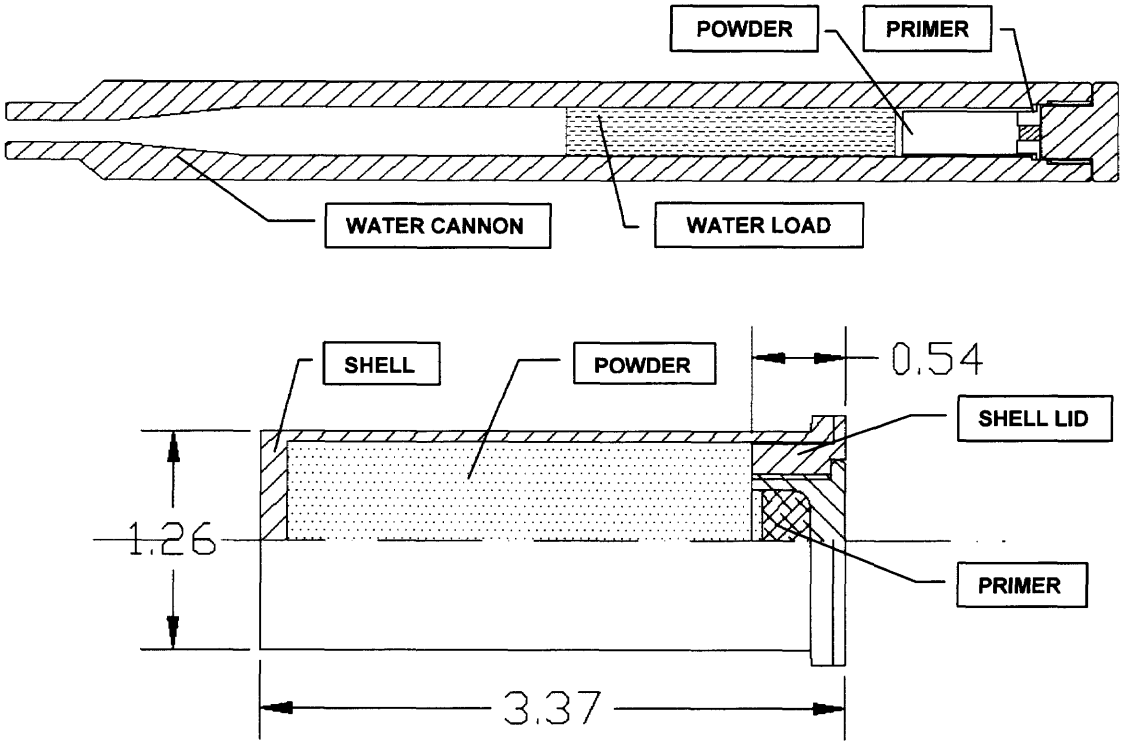

Figure 4.2 Detailed schematic of the water cannon used in the experiments.

A water cannon consists of a cylindrical barrel, tapered nozzle with cylindrical collimator at one end, and a breech with firing mechanism at the other.

Each of the manufactured devices has a barrel 400mm long and 32mm in diameter. The nozzle exit diameter is 15mm, the nozzle conic part is 70mm long, and its collimator is 75mm long. Initially the water load constituted a cylinder occupying part of the barrel, and is secured by porous rubber plugs next to the powder charge. The charge is placed at the end of the barrel in a custom made aluminum or brass shell. Electrical primers employed in Russian 30mm rapid-firing cannons were originally utilized for powder ignition. Later, percussive primers were introduced. For these two types of primers, two firing (initiating) mechanisms were designed and constructed in Donetsk National University by A.V. Kovalev. The initiating mechanisms are part of the breach that is thread-locking to the barrel (Figure 4.2 a). The igniting mechanism for electrical primers is an electrically isolated spring-loaded steel pin. The primer in the loaded cannon discharges when voltage is applied to the water cannon body and the pin. This simple and reliable ignition design has demonstrated 100% consistency in operation. However these electrical primers are used by the military and are not readily available. Thus experiments had to be carried out using regular percussive primers used in shotguns. For this an electromechanical percussive ignition mechanism was constructed. In it a solenoid-accelerated hammer strikes a pin spring-loaded against the percussion primer. The solenoid is powered by 250V capacitors charged from a 12V battery through a DC/DC converter. This schematic after several trials and improvements was working well and reliably. The utilized primers are designed for ignition of 2-3g of gunpowder in

the relatively small shotgun shell. Although the charges in the water cannon are 20-30 times larger, they were ignited well by these primers.

The device dimensions and charge schematics are shown in Figure 4.2. The nominal water load is 230g, and the powder charges range from 40g to 70g. During the experiments, different charge designs and charging methods were devised and evaluated. The desired tradeoff between charge design simplicity, manufacturing cost, reloading speed and reliability was achieved.

In order to study water slugs produced by impulsive water jet devices, several types of direct and indirect measurements can be utilized. One of them is velocity measurement of the slug's front, which in in most cases is the maximal outflow velocity of a stream produced by the water cannon. This velocity determines the maximal power delivered to the target. It also determines the water impact pressure, which, in the case of a rigid target, is higher than the dynamic pressure at subsonic velocities. Several devices

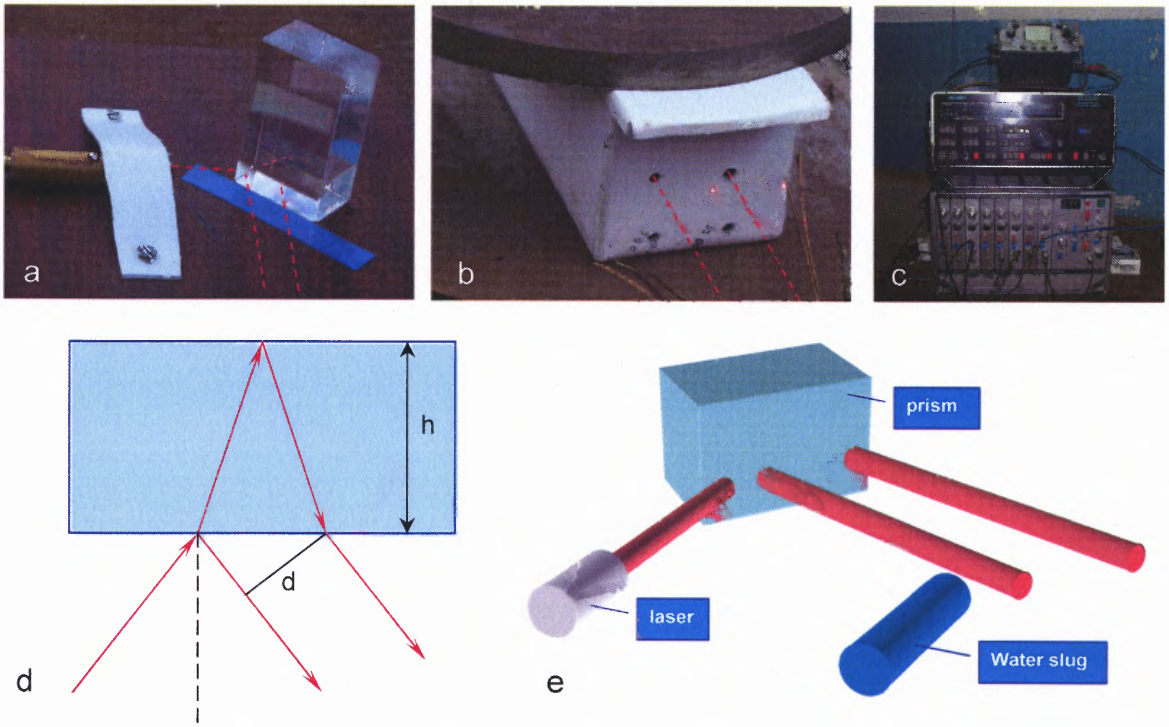

Figure 4.3 Schematic of the device for measuring water slug's head velocity.

measuring the slug's front velocity were designed, constructed and tested. They are all based on measurement of the duration the slug's front traveling over a fixed distance. The duration-to-distance ratio is equal to the front velocity. A schematic and photograph of one of the devices is shown in Figure 4.3. It consists of two parts. One part generates two parallel laser beams perpendicularly crossing the water cannon axis at the nozzle exit. The other part detects the beams' light with two photodiodes. When a moving water slug intercepts the laser beams one after the other the signals from the photodiodes is registered by two channels of a digital oscilloscope. In the experiments the photodiodes were connected to DataLab's DL 2B08 multichannel recorder and stored on a magnetic medium with DL 1080, and the signals were output to C1-73 oscilloscope for visual evaluation. (Figure 4.3c)

Special photodiodes were implemented in order to minimize the raise time on the circuits' outputs. In the case of anemometer shown in Figure 4.3 the signals from the sensors were fed to the DataLab's DL 2B08 multichannel recorder and stored on a magnetic medium with DL 1080, and the signals were output to C1-73 oscilloscope for visual evaluation. A two channel 20MHz digital oscilloscope Fluke was used with the anemometer shown in figure 4.4.

The parallel light beams were obtained by splitting a semiconductor laser beam with a splitting prism. (Figure 4.3a) This arrangement proved to be not only reliable and easy to set up in a field, but also generates beams with identical cross-sectional profiles, assuring the accuracy of the measurements. The lasers at the time available for experiments generated low-quality beams: they couldn't be well focused and had irregular forms of cross-sections of about 2mm in diameter. So when the slug intercepts

the beams with identical cross-sectional shape, the shapes of the signal ramps sent to oscilloscope are identical, and the signals may only differ in absolute value. This enables exact matching of the signals without additional calibration and increases measurement accuracy. The distance between the beams is calculated by the formula:

$$d = 2h\cos\alpha \cdot \tan\left(\arcsin\left(\frac{\sin\alpha}{n}\right)\right) \qquad (4.1)$$

A part detecting the laser beams has two high-speed photodiodes placed in a relatively large long box with two openings matching the beam diameters. This eliminates interference of the surrounding diffusive daylight. Additional filtering can be provided by inserting inside partition walls with openings for beams.

Another device for measuring the slug's front velocity was designed and constructed at Donetsk National University. This device has a built-in timer and employs parallel metal wires to detect the water slug. When the water slug impacts and breaks the wires an electrical current passing through them is interrupted. These interruptions of the current serve as a signal to start and stop the built in timer. The design has one peculiarity: the detecting wires should have precisely identical tension for accurate measurement of the velocity. With uncontrolled tension, the accuracy significantly decreases due to different displacement of the wires when they break.

The device shown in Figure 4.4 employs both detecting techniques: light and conducting electrodes. In order to assure precise control of the electrodes breaking and eliminate the need for precise tension control, graphite pins were utilized instead of metal wires. Placed without any tension, the electrodes break under a fraction of a millimeter displacement. This assures high accuracy of slug position detection. Instead of lasers a more simple arrangement involving two focusing IR LEDs was used for light emission.

Phototransistors with built-in amplifiers were used for light detection. Good strength and focusing of LEDs and a short distance between LEDs and phototransistors eliminate the need for special shielding of ambient daylight.

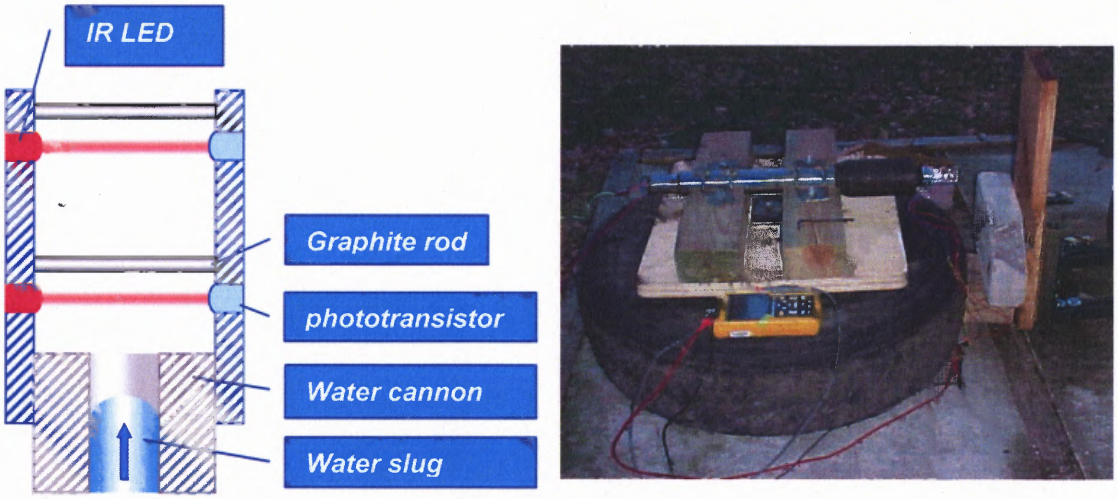

Figure 4.4 Water slug head's front velocimeter setup.
IR LEDs and amplified phototransistors from a photo-interrupter are employed in the sensor. The sensor also has two 1.5mm graphite rods installed. The signals from the graphite and phototransistors are fed to a two-channel oscilloscope.

Each pair of the front detectors – phototransistors and graphite electrodes – were connected to a two channel 20 MHz digital oscilloscope Fluke 123 through a voltage divider. This allows detecting two ramps from two detectors, phototransistors or electrodes, on each single channel. However, this velocity measuring device has one limitation, it cannot measure high-power waterslugs. Previous version setups were destroyed in experiments. High-speed filming of the slug travel in air has revealed the expansion of the slug and shock wave generation at the slug exiting the nozzle.

The filming was done in the water jet technology laboratory, NJIT using the digital camera Phantom V7.0. The filming was done at 50-100K fps with 1-3μs exposure and a resolution of 100-208 pixels along the frame. Figure 4.5 depicts one of the experiments filmed at 230g of water load, and 70g of powder charge producing a slug with a front velocity of 1600m/s.

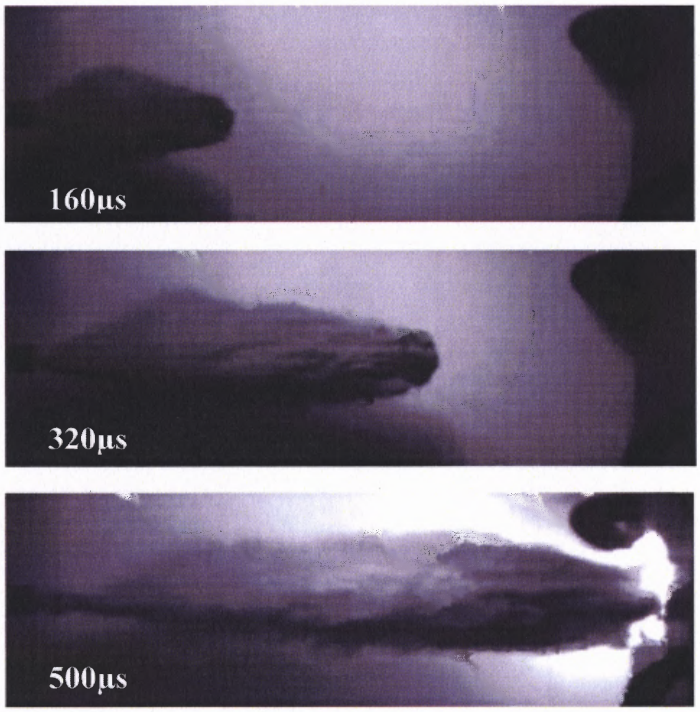

Figure 4.5 Captions from the high-speed filming.
Water load – 230g; Charge – 70g; Velocity of the slug's front – 1600m/s.

The filming clearly depicts expansion of the slug at the exit of the nozzle that destroyed the velocimeter. An interesting effect is observed at impact on the steel plate. We attribute it to combustion of a porous rubber plug containing the water in the barrel during loading.

High-speed water slugs were tested to neutralize explosive setups involving standard ordinance and improvised explosive setups. The experimental study of the water cannon involved the piercing of metal and crushing of brittle and viscous material as

well. The velocity of the slug was measured by a custom-made anemometer and via high-speed filming of the slug's propagation in air. The filming was done using a digital high-speed camera Phantom V7.0. The filming was done at 50-100K fps with exposure 1-3μs and resolution of 100-208 pixels along the frame. The custom-made anemometers are described below. The obtained water velocity ranged from 1,250m/s in the case of 40g powder charge to 1,600m/s in the case of 70g powder charge.

4.2 Demolition Experiments With Water Cannon

The destructive potential of high-speed water slugs was recognized long ago. Industrial-scale water extruders were built for demolition tasks and successfully tested in the mining industry. The potential of the manufactured cannon had to be investigated on diverse targets. A series of experiments (Figures 4.6 – 4.10) were run in collaboration with Donetsk National University in Donetsk and in Kiev, Ukraine.

The process of the demolition of the concrete block is shown in Figure 4.6b. The results of the impact are depicted in Figure 4.6c. The dimensions of the concrete block in this experiment were 26 x 30 x 40cm while its relative strength was 300-500.

a b c

Figure 4.6 Destruction of a 26x30x40 cm scale 300-500 concrete block:
a) set-up of the experiment, b) the moment of destruction, c) largest piece of the block.

Demolition of the armored concrete, which is a major construction material, is depicted in Figs 4.7 – 4.10. Two concrete plates (Figure 4.7) of hardness of more than 400 were used. The standoff distance from the closest plate was 2 cm. The closest plate was 13cm thick. A hole of 5-8 cm in diameter was created in the first plate. The second plate was located at a distance of 12 cm from the first one and was not affected by the water slug. This demonstrates the effect of the standoff distance on the results of the impact. In another experiment the concrete block of 16 cm had a hardness of 400. The results of water impact are shown in Figure 4.8.

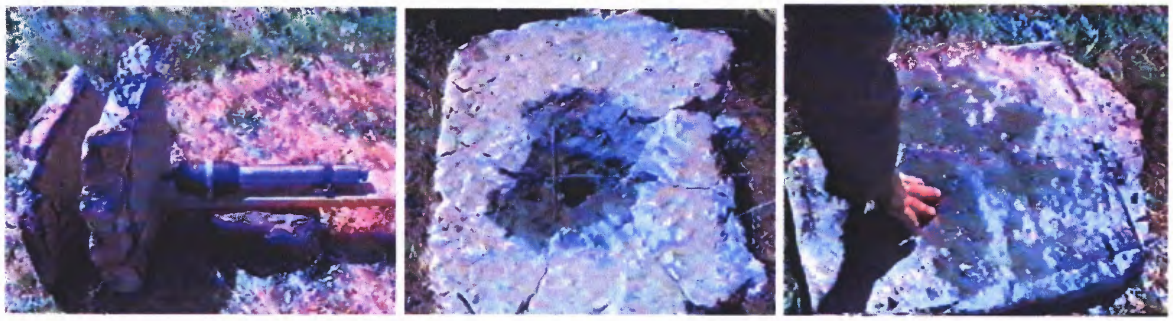

a b c

Figure 4.7 Destruction of concrete brand 300-500 plates:
a) set up of the experiment,
b) result of interaction with the first plate,
c) result of interaction with the second plate.

a b c

Figure 4.8 Destruction of concrete brand 300-500 block:
a) set up of the experiment,
b), c) results of water-concrete interaction.

The ability of a water slug to penetrate steel and still possess a significant amount of power is demonstrated by Figure 4.9. In this experiment, a concrete block of 14cm protected by the steel plate having thickness of 6 mm was used. The shape of a steel plate kept the standoff distance at 3cm. The results of destruction are shown in the same figures.

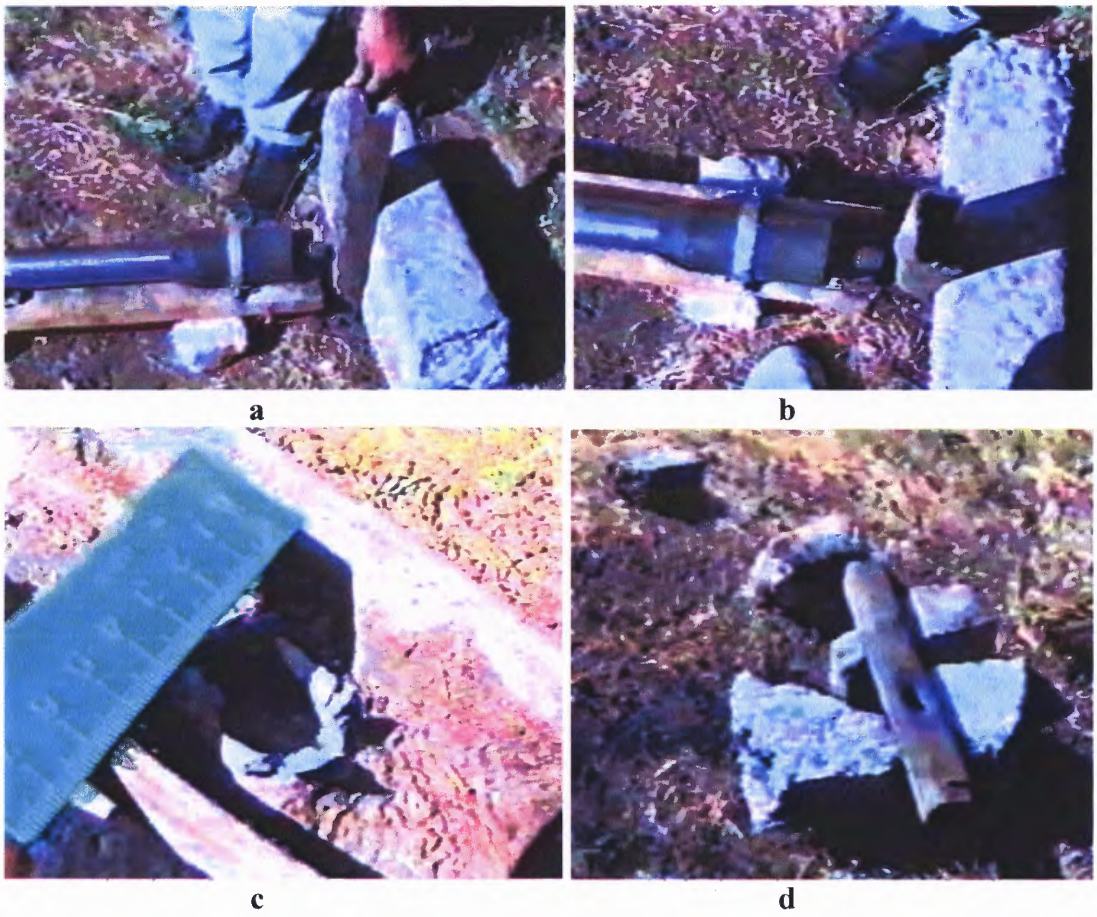

Figure 4.9 Destruction of concrete brand 300-500 block with a 6 mm steel plate
a), b) set up of the experiment,
c), d) results of the shot.

Steel penetration experiments were conducted with an enlarged rifle gunpowder load of 70 grams. The water load remained 230g. Outflow velocity at this charge and load is 1600m/s.(Figure 4.5) 14.4 mm of hot-rolled steel in three 4.8mm plates placed together were penetrated by water (Figure 4.10).

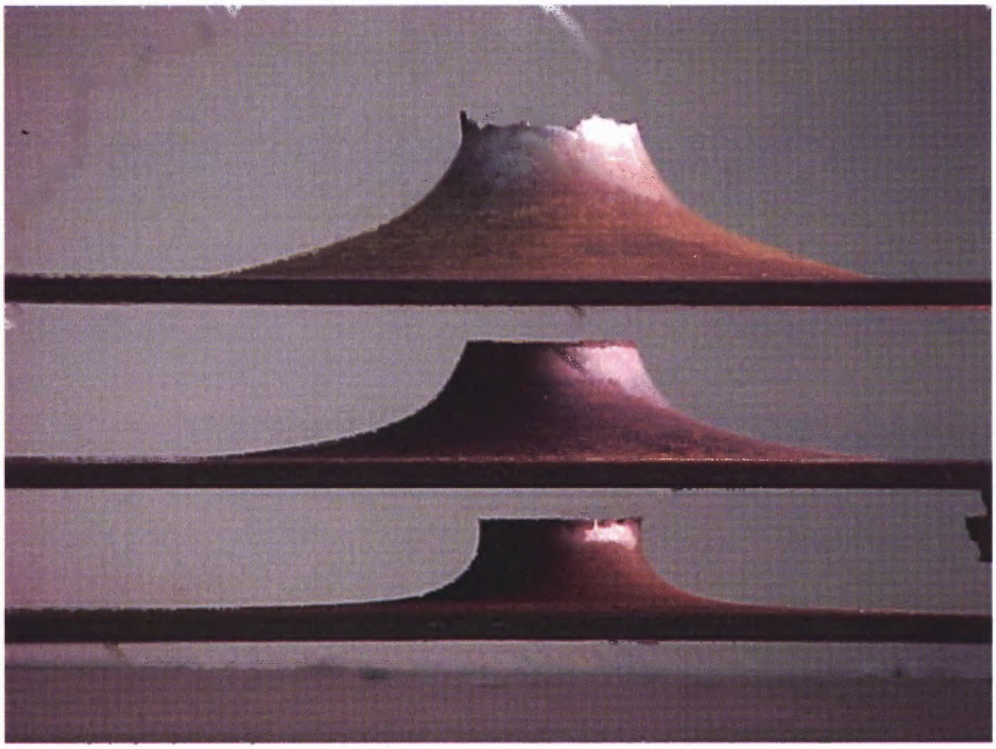

Figure 4.10 Penetration of three placed together 4.8mm plates with 240g of water using 60g of rifle powder.

A series of concrete demolition experiments were performed with a reduced powder load of 30g of fast burning pistol powder producing 1000-1100 m/s water slugs. These experiments were conducted by NJIT, Donetsk National University in Kiev at the Paton Institute of Welding. The experiments demonstrated significantly smaller damage to the tested concrete blocks. (Figure 4.10) It was concluded that the water slug should have velocity above some threshold to remove material effectively. It was concluded that the minimum critical slug velocity in case of concrete demolition is about 1200 m/s.

a b

Figure 4.11 Results of two consequent shots to a butt of an armored concrete block with reduced powder charge (30g of powder, 230g of water).

The performed experiments provided understanding of the feasibility of brittle material demolition and plastic material penetration by high-speed water slugs. In order to understand the mechanism of this process, and most of all optimize the performance of the water cannon, more experiments as well as a numerical study are required.

4.3 Explosive Setups Neutralization Experiments.

Another important application of high-speed water slugs is the neutralization of explosive devices without their detonation. This ability of a water slug is utilized in instruments termed disruptors. Disruptors are smooth-bore guns firing water slugs or rigid projectiles. The produced slugs have a velocity of 300-400m/s. Slugs at such velocities are capable of neutralizing case-less or soft-case explosive devices. These are usually improvised explosive devices (IED), non-regular non-serial arms created by individuals for terrorist and other criminal purposes. Police bomb squads around the world successfully use disrupters for soft-case IED neutralization. However the Army doesn't employ these disruptors in demining operations. Underground mines or those with a strong casing are

not affected by a relatively slow water stream. Meanwhile the problem of safe mine neutralization is far from being resolved.

The problem of landmine clearance is a very urgent one. There are more than 100 million landmines laid in the ground. In Cambodia 25-40% of fertile land is mined. Landmines maim and kill about 20,000 people every year (ICBL), one third of them are children (UNICEF). About 80% of the landmines' victims are civilians (ICBL).

Mine clearance operations have two major challenges, mine detection and mine neutralization. Mine detection is a dangerous tedious task, complicated by hundreds of false alarms per each mine found. Mine neutralization is risky as well. Most of the neutralization is done manually by removing mines from the ground, taking out the detonators and destroying them in bulk by a donor charge in a nearby pit. Some mines are equipped with non-disturbance fuses and booby-traps, which make mine neutralization so risky. The policy of the U.S. Department of Defense is that the hostile mine should be neutralized in place by a donor charge. This technique is the safest for an operator but it is considered impractical by most of deminers. The explosion scatters the mine charge and metal parts over a large area. The mine charge scattered over a minefield makes use of dogs impossible for a week, and the scattered metal fragments result in numerous false alarms.

The studied water cannon has produced water slugs with velocities up to 1600m/s. These slugs were experimentally evaluated to be capable of to penetrating topsoil for at least 1m, penetrating 15mm of steel, and going through concrete blocks.

A series of explosive neutralization experiments were done by the author and Drs. Atanov, Semko and Kovalev. Figure 4.12 depicts disruption of a simulated large mine by the water cannon loaded with 230 g of water and 40g of VT rifle powder. The simulated mine was a 40-50kg of transparent silicon-type material enclosed in a steel cylindrical container 50 cm high and 30cm in radius. A 4-mm steel plate shielded the mine. The container was completely destroyed (Figure 4.12c) with its contents dispersed over an area of 15 meters in radius (Figure 4.12b).

a b c

Figure 4.12 Destruction of an explosive assembly simulation.
a) set up of the experiment,
b) waterslug scatters the contents of the container,
c) results of the shot: 5cm hole in the 4mm steel plate, bottom part of the container.

Neutralization of live explosive setups with the water cannon was studied with the assistance of the Donetsk MVD bomb squad.

a b c

Figure 4.13 Successful neutralization of a soft-case explosive setup.

The first target was a setup in a soft container and consisted of 150g of trinitrotoluene (TNT), an internal detonator, and an anti-disturbance fuse making it non-dischargeable. The device was successfully neutralized without charge detonation. (Figure 4.13)

The next device had the same principle of operation and the same load of explosive, however, the enclosure was a 4mm-walled steel tube with 6mm steel lids. The cannon was aimed at the TNT charge. The setup was neutralized with detonation of the explosive charge. (Figure 4.14)

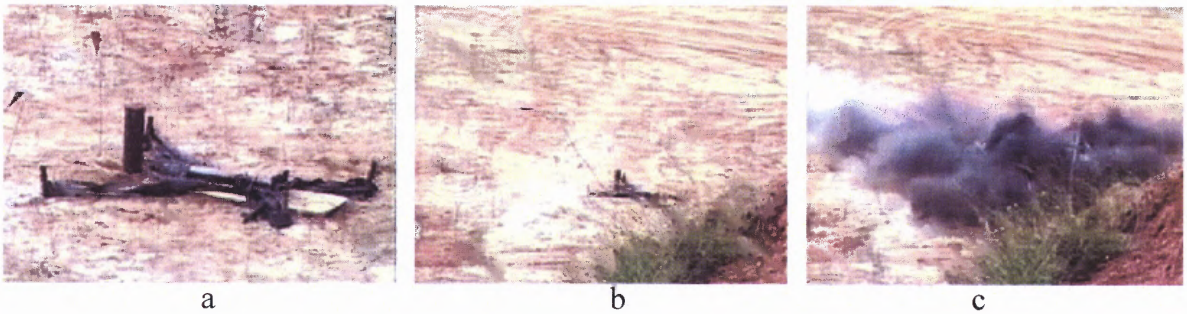

a b c

Figure 4.14 Experiment on neutralization of a hard-case explosive setup.
a), b) The setup and the water cannon installation. c) Explosion of the setup.

The next target was a Russian offensive hand grenade RGD-5 (Figure 4.14a). It has 110g of TNT charge, and with UZRGM fuse weights 310g. The grenade was neutralized with detonation of the charge (Figures. 4.15b, 4.16c). Most likely the detonation happened due to discharge of initiation explosives in the fuse. A UZRGM fuse contains lead trinitoresorcinate above lead azide. These substances are extremely sensitive to mechanical and thermal impacts, while TNT is very stable to mechanical influences.

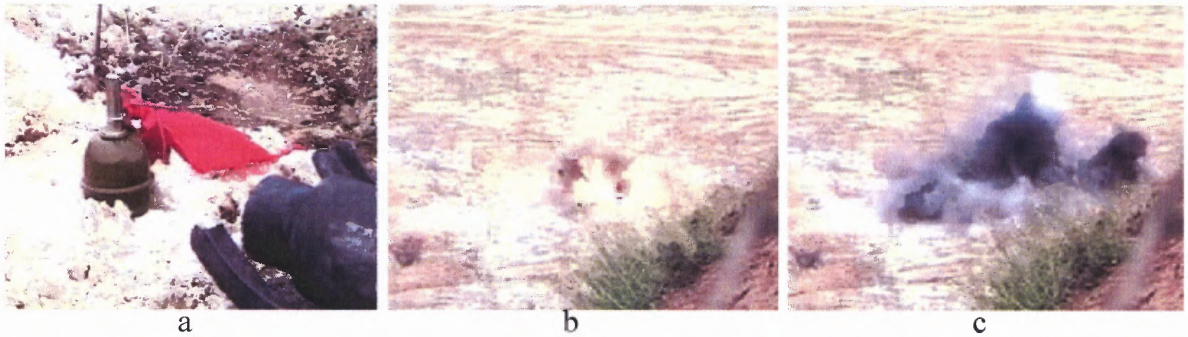

a b c

Figure 4.15 Experiment on neutralization of an offensive hand grenade.
a) The initial setup, b) Moment of explosion, c) After the explosion.

Explosive setups encountered in practice by bomb squads are very diverse. Many factors should be taken into account when attempting to neutralize one using water slugs:

- Type of explosive material used, its physical state, presence of admixtures
- Casing of the explosive device: its material, thickness, form, fragmentation ballistic elements
- Type of detonator; its positioning type (external / internal) and location
- Utilized sensors, booby traps, non-disturbance fuses
- Orientation of the device

Different explosives have very different sensitivity to a mechanical impact. Most of them are very sensitive. The addition of the sand powder or grinded glass dramatically increases mine sensitivity. In contrast, sensitivity is lowered by addition of paraffin or stearin. In some cases explosives sensitivity significantly varies with temperature. (E. Petrenko, 2002)

Casing material, its form, wall thickness and positioning of explosive in it define how the slug penetrates it, and what is the impact velocity. It determines whether the water directly impacts the charge or it acts on the charge via the deforming case. While

water is a good phlegmatizer, a rough internal case surface increases the probability of detonation. (E. Petrenko, 2002). Thin-walled cases can be ruptured without transmitting sufficient disturbance to a detonator containing sensitive explosives like lead azide or fulminate of mercury. Also, a delay in disturbance transmitting can be sufficient for scattering the main charge before the detonator or a non-disturbance fuse setoff. Thick walled rigid cases are good transmitters of waves generated at impact. In the case of firmly fixed detonator in a hard case, it triggers before the charge is scattered by the water slug.

If the detonator is located in the charge without direct contact with the casing, it is set off by the first compression wave generated by the slug impact.

Non-disturbance fuses are installed in mines and IED to prevent demining. In most regular mines the initiation unit provides a delay of 200-300msafter a signal from a non-disturbance fuse. So if the main charge is sufficiently scattered within this time period and the detonator didn't initiate, the mine will be neutralized without detonation.

4.4 Concluding Remarks

The experimental study of the water projectiles produced by the constructed water cannons has demonstrated high potential in demolition, metal piercing and explosives neutralization. Very low performance of slower water projectiles suggests the possibility of qualitatively different results at even higher velocities. For this, new devices have to be designed and constructed.

CHAPTER 5

NUMERICAL MODELING OF WATER CANNON OPERATION

5.1 Objective

Numerical modeling of processes occurring in the water cannon is essential for the following tasks:

- Design of a water cannon device optimal for a particular operation or a set of operations
- Experimental study of slug-target interaction

Design of a water cannon device requires a) selection of optimal parameters of the new device, b) distribution of the pressure exerted on the device walls, c) recoil of a new device shot.

For the experimental study of the projectile-target interaction, the parameters of the impacting projectile should be known. Measurement of the velocity distribution within a projectile is a very complicated task, requiring expensive state-of-the-art equipment. Meanwhile, a projectile's properties at the exit of the nozzle can be determined by numerical modeling via the initial conditions such as powder charge and water load.

Numerical modeling of the powder water cannon's internal ballistics consists of two bounded problems – gunpowder combustion modeling and modeling of water flow inside the cannon. While it is the water flow that determines the pressure and velocity fields, powder combustion determines the gas pressure exerted on the water load and, thus, defines its acceleration in the barrel and its transformation in the nozzle.

5.2 Powder Combustion Modeling

In the performed experiments energy, the water acceleration in the water cannon is obtained via gunpowder combustion. Thus, the pressure of the combustion products, $p_g(t)$, determines the boundary conditions at the rear surface of the water load. Modeling $p_g(t)$ as an adiabatic expansion of the a reacting gunpowder products provides a good approximation for small amounts of fast powders accelerating a relatively heavy projectile. Such approximation accuracy is sufficient for modeling heavy piston acceleration of a water extruder. However, in most of the water cannon experiments the employed gunpowder had a much slower combustion rate due to large grain size. Also the mass of the powder charge is comparable to the water load mass. Thus, another model for $p_g(t)$ is required. It has to take into account the rate of gunpowder combustion. A Coppock model (B.V. Orlov, 1974), commonly used in solving internal ballistic problems, was utilized for powder combustion modeling in the water cannon. The model is based on the following assumptions:

- all powder grains are instantaneously set on fire
- powder combustion is an adiabatic process
- the process is uniform and occurs on the surface of a grain
- chemical composition of combustion products is constant and uniform in space
- thermodynamic properties of the combustion products are approximated by the simplified Van der Waals equation:

$$p_g\,(v\ -\alpha) = q\,(k-1)\,T/T_0 \tag{5.1}$$

At pressures less than 500 MPa the covolume α can be assumed to be constant and equal to 0.001 m³/kg. The linear velocity of combustion front propagation in a powder grain is proportional to the pressure of the powder gases.

$$u_p = u_1 p_g \tag{5.2}$$

The rate of combustion products generation, J_g, is determined by the surface area of an average powder grain, combustion velocity and density of the powder matter ρ_p.

$$J_g = s\rho_p u_p \tag{5.3}$$

The energy balance equation is.

$$qJ_g = \frac{k}{k-1} p_g \frac{dV}{dt} + \frac{V}{k-1}\frac{dp_g}{dt} \tag{5.4}$$

where V – is the gas volume, increasing due to water load movement and reduction of solid powder volume. Covolume should be taken into account.

$$\frac{dV}{dt} = J_g\left(\frac{1}{\rho_p} - \alpha\right) + u_p F \tag{5.5}$$

The above considerations result in the following quasistationary system of equations:

$$\frac{dz}{dt} = \frac{u_1}{h_1} p_g \tag{5.6a}$$

$$J_g = m_{p0}\chi_1\sigma(z)\frac{dz}{dt} \tag{5.6b}$$

$$\frac{dV_g}{dt} = u_g F_c + \left(1/\rho_p - \alpha\right)J_g \tag{5.6c}$$

$$\frac{dp_g}{dt} = \frac{1}{V_g}\left[(k-1)qJ_g - p_g\left(1/\rho_p - \alpha\right)J_g\right] \tag{5.6d}$$

$$\sigma(t) = z + 2\lambda_1 z + 3\mu_1 z^2 \tag{5.6e}$$

Here the equation (5.6a) defines the rate of the reduction of the linear grain size, which is assumed to be proportional to the pressure of the combustion products. Equation (5.6b) yields the rate of the generation of the combustion products, which is proportional to the free surface of the powder grains. The rate of change of the volume of combustion products is determined by the equation 5.6c. Equation (5.6d) determines the energy balance of the process.

This system of equations (5.6) was integrated simultaneously with calculations of the fluid flow in the cannon using the second-order Euler method. At each time-step analysis of the water flow and the value of p_g was determined and used at the time-step to define the boundary conditions on the gas-water interface at the time-step.

The rifle powder used in the experiments has cylindrical grains without cavities. The geometry constants for this grain shape are

$$\chi_1 = 2 + \frac{R}{c}, \quad \lambda_1 = -\frac{c+2R}{2c+R}, \quad \mu_1 = \frac{R}{2c+R} \tag{5.7}$$

where the powder grain length is c, and its radius R.

The code for integration of system (5.6) was written and included in the program for modeling fluid acceleration and development in the water cannon.

5.3 Projectile Formation Modeling

Water flow within a cannon is modeled by the Navier-Stokes equations and the water constitutive equation. However this system of equations is too complicated to solve in general. Process peculiarities should be taken into account in order to simplify these equations to make solution practical.

The studied experimental water cannon and similar devices described in the introduction have the following ranges of parameters.

- Outflow water velocity: 700 – 2000 m/s
- Average water velocity in the barrel: 200 – 500 m/s
- Nozzle exit diameter: 10 – 20mm
- Water pressure: up to 1,000 MPa
- Angle of nozzle convergence: 7 – 10 degrees

These parameters values suggest plausible assumptions that can be used to reduce the general system of equations. The small angle of nozzle convergence enables the reduction of the problem to the 1-D case. High velocities and relatively large characteristic dimensions yield a high a Reynolds number:

$$\mathrm{Re} = \frac{VD}{\nu} = 1000\mathrm{m/s} * 10^{-2}\mathrm{m}/10^{-3}\mathrm{s/m^2} = 10^4$$

Thus it can be assumed the flow is inviscid. At high pressures attained in the cannon, water flow cannot be considered to be incompressible. A pressure of 1,000MPa results in 10% of water volume reduction. The short time duration and the absence of strong shock waves make it possible to assume that the flow is isentropic.

The above assumptions were employed by Atanov (Atanov, 1987, Atanov, 1977) to obtain the following system of equations:

$$\frac{\partial u}{\partial t} + u\frac{\partial u}{\partial x} = -\frac{1}{\rho}\frac{\partial P}{\partial x} \tag{5.8a}$$

$$\frac{\partial \rho}{\partial t} + \rho\frac{\partial u}{\partial x} + u\left(\frac{\partial \rho}{\partial x} + \rho\frac{1}{F}\frac{\partial F}{\partial x}\right) = 0 \tag{5.8b}$$

$$\frac{P+B}{\rho^n} = const \tag{5.8c}$$

These are 1-D dynamic equations of the momentum and mass balance and the isentropic state equation. Boundary conditions for equations (5.8) are obtained from the principle of operation of the studied experimental water cannon. Initial velocities and pressure in the barrel are assumed to be zero. The pressure at the gas-liquid interface in the course of the process is equal to the pressure of the combustion products, while the pressure at the free surface separating the liquid and the atmosphere is assumed to be zero. In the performed computations the entrance of the nozzle is taken to be the origin of the space with coordinate x. The initial time is the moment of powder ignition. So the initial and the boundary conditions of the system (5.8) can be written as

$$u\,(x,\,0)=0,\ \rho(x,\,0)=\rho_0,\ P(x,\,0)=0,\ P(-L_{brl},\,0)=P_g(0),\ x\in(-L_{brl}\,;\,-L_{brl}+L), \quad (5.9a)$$

$$P(x_{gas}(t),\,t)=P_g(t),\ P(x_{free}(t),\,t)=0 \quad (5.9b)$$

Where $x_{gas}(t)$ and $x_{free}(t)$ are the coordinates of the gass-water interface and the free surface. Using the isentropic equation (5.8c), the number of variables in the first two equations can be reduced from three to two and the system (5.8) can be reduced to the form

$$\frac{\partial u}{\partial t}+\frac{\partial}{\partial x}\left(\frac{u^2}{2}+\frac{\rho^{n-1}}{n-1}\right)=0 \quad (5.10a)$$

$$\frac{\partial u}{\partial t}\rho F+\frac{\partial}{\partial x}uF=0 \quad (5.10b)$$

Equations (5.10) are written in non-dimensional form. The sound speed in water and water density at normal conditions and barrel length were used for scaling. Integration of system (5.10) over an arbitrary domain in the x-t space yields:

$$\iint\left[\frac{\partial u}{\partial t}+\frac{\partial}{\partial x}\left(\frac{u^2}{2}+\frac{\rho^{n-1}}{n-1}\right)\right]dxdt=0 \quad (5.11a)$$

$$\iint\left[\frac{\partial u}{\partial t}\rho F+\frac{\partial}{\partial x}uF\right]dxdt=0 \tag{5.11b}$$

Here A is the area of integration. Using Green's formula we can rewrite system (5.11) as

$$\oint\left[udx-\left(\frac{u^2}{2}+\frac{\rho^{n-1}}{n-1}\right)dt\right]=0 \tag{5.12a}$$

$$\oint[\rho Fdx-u\rho Fdt]=0 \tag{5.12b}$$

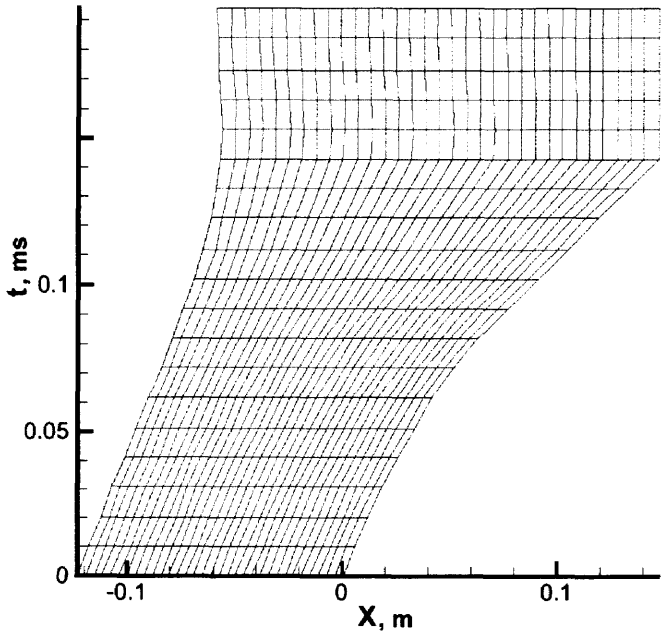

Figure 5.1 Schematic of the mesh

The computational procedure involved numerical solution of the system (5.12). The technique is based on the finite difference method while the method of characteristics is used to relate fluid properties at the t and $t+\Delta t$ intervals. This method was suggested by Godunov (Godunov, 1976) and carries his name. The 1-D time-space computational domain was approximated by a trapezoidal grid with a constant number of x-steps equal at each time instance (Figure 5.1). The schematic of an individual grid cell is shown in Figure 5.2. Here horizontal lines represent the state of water at time instances

t and $t+dt$. As the projectile moves within the converging nozzle its length changes and so does the lengths of horizontal sides of a cell.

The distribution of the velocity and density in the projectile are approximated by step functions of x that change over time. Then a boundary between two cells, that are nodes in Figures 5.2 and 5.3, constitutes a discontinuity of u and p functions. The collapse of such a discontinuity results in the creation of two waves moving along two characteristics. Riemannian invariants are used to find the state of the fluid between the two waves:

$$\frac{dx}{dt} = u \pm \rho^{\frac{n-1}{2}} \tag{5.13a}$$

$$u \pm \frac{2}{n-1}\rho^{\frac{n-1}{2}} = const \tag{5.13b}$$

Where u and ρ are constant on the lateral sides 1-2 and 4-3. These values of u and

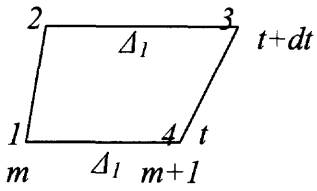

Figure 5.2 A grid cell schematic

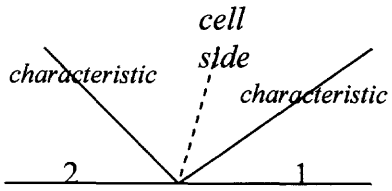

Figure 5.3. Schematic for eq. (5.13)

ρ on the lateral sides of each cell are calculated from discontinuity decomposition using the characteristic equations: the values at the following instance of time $(t+\tau)$ are to be found.

A point of discontinuity, for any an every node of the mesh, is a common point of the characteristic of the first family, of the characteristic of the second family and the lateral side of the grid that the point belongs to. Thus, from (5.13) the following equations hold:

$$u_1 - \frac{2}{n-1}\rho_1^{\frac{n-1}{2}} = U - \frac{2}{n-1}Ro^{\frac{n-1}{2}} \tag{5.14a}$$

$$u_2 - \frac{2}{n-1}\rho_2^{\frac{n-1}{2}} = U - \frac{2}{n-1}Ro^{\frac{n-1}{2}} \tag{5.14b}$$

Using system (5.14) the value of velocity and density at the lateral sides, U and Ro, can be determined as follows. For this dt should be sufficiently small so that characteristics do not intersect the lateral sides.

$$U = \frac{1}{2}\left[u_1 + u_2 - \frac{2}{n-1}\left(\rho_1^{\frac{n-1}{2}} - \rho_2^{\frac{n-1}{2}}\right)\right] \tag{5.15a}$$

$$Ro = \left[-\frac{n-1}{4}(u_1 - u_2) + \frac{1}{2}\left(\rho_1^{\frac{n-1}{2}} + \rho_2^{\frac{n-1}{2}}\right)\right]^{\frac{2}{n-1}} \tag{5.15b}$$

This holds if dt is sufficiently small so that characteristics do not intersect the lateral sides. Using values of U and Ro obtained in (5.16) we can relate u and ρ at the time instances t and $t+dt$ (Atanov, 1987, Voitsehovskiy et al., 1971):

$$u^{m+1/2} = \frac{1}{\Delta_1}\left[u_{m+1/2}\Delta_2 - dt\left(c_{m+1} - c_m - U_{m+1}W_{m+1} + U_m W_m\right)\right] \tag{5.16a}$$

$$\rho^{m+1/2} = \frac{1}{F_u\Delta_1}\left[F_l\rho_{n+1/2}\Delta_2 - dt\left((RUF)_{m+1} - (RUF)_m - (RFW)_m + (RFW)_m\right)\right] \tag{5.16b}$$

$$c_i = \frac{U_i^2}{2} + \frac{Ro_i^{n-1}}{n-1} \tag{5.16c}$$

$$W_m = \left(x^m - x_m\right)/dt \tag{5.16d}$$

Where:

F_l, F_u, F_m, and F_{m+1} are the average values of nozzle cross-section area corresponding to the sides of a cell *1-4*, *2-3*, *1-2* and *3-4* respectively.

A computer code has been developed to simulate the water cannon operation using this scheme (equations 5.15 and 5.16). A block of code modeling gunpowder combustion was also included in the program.

The model and the program were experimentally validated by measuring the projectile's front velocity with custom-built anemometers, a high-speed camera and a ballistic pendulum.

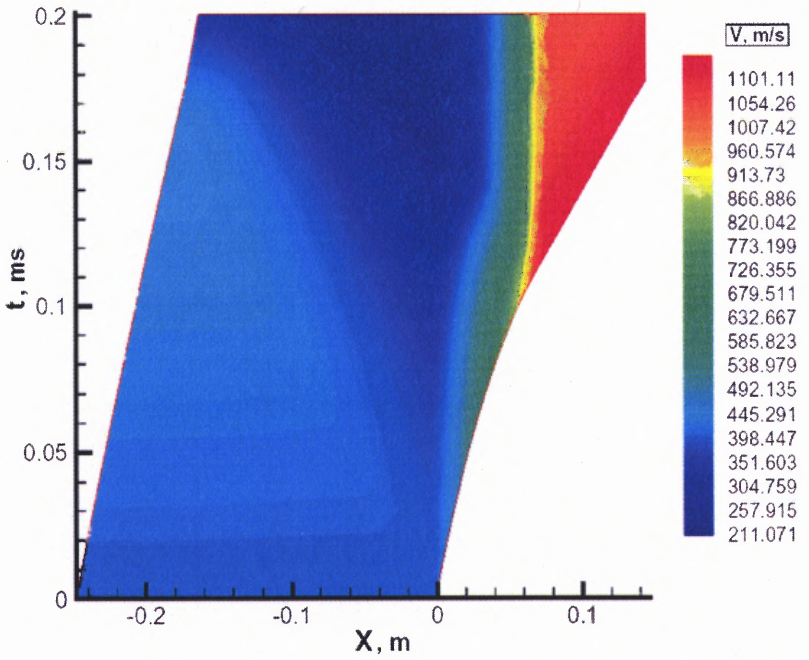

Figure 5.4 Distribution of water velocity during the process of 200g slug flow in the nozzle. Point of origin is shifted up to the moment of inflow.

Formation of the water projectile in the nozzle is shown in Figures 5.4 and 5.5. At time $t=0$ the velocity distribution in the barrel is uniform. The kinetic energy within the projectile is redistributed so that the front part is accelerated by means of deceleration of the rest of the projectile. This is the main principle of the water cannon operation that is not sustained in stationary systems.

The results of computation were used to evaluate correlations between the design and operational parameters of the water cannon. The computational analysis was carried out for processes occuring in the studied water cannon device. The principle parameters of this water cannon were as follows: barrel length – 70 cm, length of the nozzle – 7 cm,

collimator length – 7.5 cm, barrel diameter – 32 mm, nozzle exit diameter – 15 mm, water load – 200 g, powder charge – 40 g.

The charts in Figures 5.5-5.7 show the change of outflow velocity in time. During the course of firing the maximum projectile velocity is maintained during roughly 0.2 ms and then rapidly drops. Thus the velocity of the projectile is non-uniform along its length. The uneven velocity distribution within the projectile brings about its decomposition, which is the main reason of short operating standoff distance for water cannons.

Front part of the projectile, where the water velocity is more than 0.85 of the

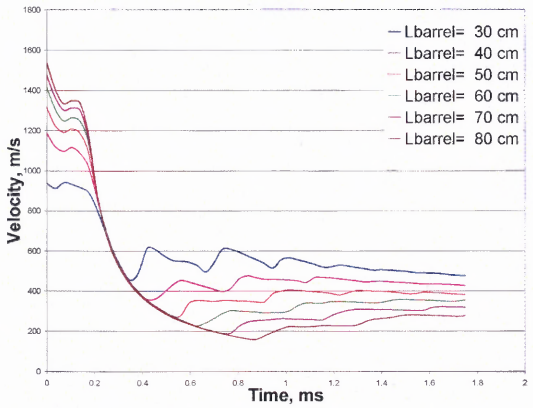

Figure 5.5 Outflow velocity vs. time at different barrel lengths

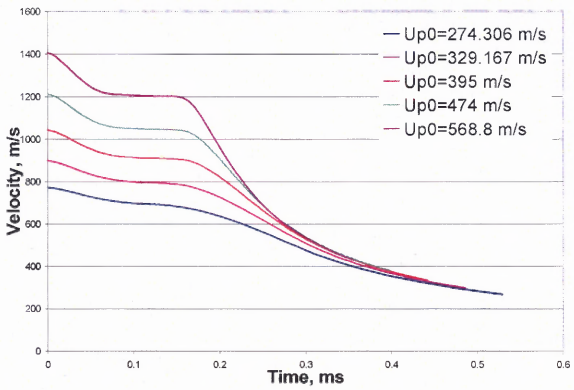

Figure 5.6 Outflow velocity vs. time at different velocities of the slug inflow in to the nozzle

maximum is termed the projectile head. The principle part of material removal in the impact zone is due to the interaction of the projectile head and the substrate.

Observing the chart in Figure 5.5, one will notice that the increase of the barrel lengths results in an increase in the difference of the velocity of the projectile head and the rest of the projectile water. Reduction of the barrel length results in a process similar to the extrusion of water, while an increase in length brings about energy redistribution within the projectile.

Water acceleration in the nozzle is determined by the kinetic energy of the water entering the nozzle and also by the pressure of the combustion products. In order to evaluate the contribution of each of the factors playing roles in water acceleration, the outflow velocity was computed at zero gas pressure in the cannon but different velocities of the projectile before entering the nozzle. The results of computations are shown in Figure 5.6.

Figure 5.7 shows the effect of the water load on the time velocity distribution. This chart demonstrates how the water load mass affects the produced projectile. The effect of the pressure is depicted by the charts in Figure 5.9. The gas pressure shown in this chart changes dramatically (from 0 to almost 200MPa). At the same time the velocity of the head changes by 20%, while the velocity of the tail practically doesn't change.

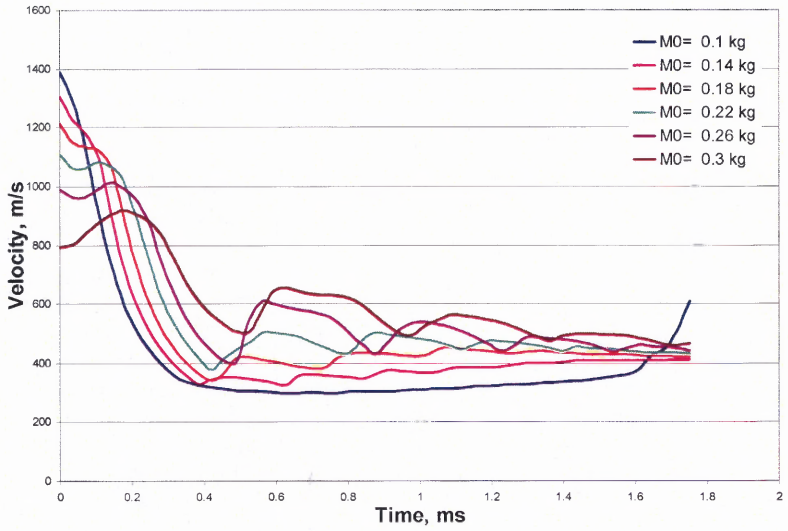

Figure 5.7 Outflow velocity vs. time at different water loads.

Comparison of the charts in Figures 5.5, 5.6, 5.7 and 5.9 shows that the gas pressure and the kinetic energy of the projectile at the entrance of the nozzle determine behavior of the head of the projectile but insignificantly effect its tail. At the same time the length of the barrel and water load determine velocities of both the head and tail.

Because the result of projectile-target interaction is mostly determined by the

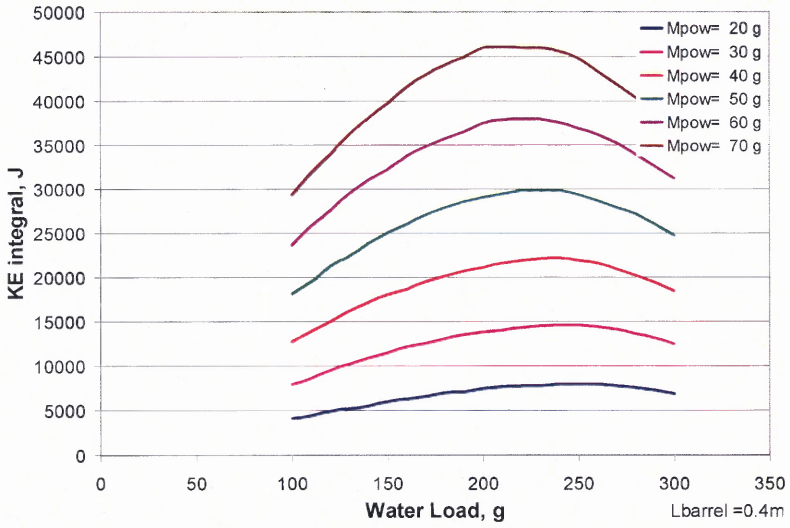

Figure 5.8 Slug kinetic energy integral vs. water load at different gunpowder charges.

projectile head rather than the tail, the effect of process conditions on the energy of the head was also investigated. Effect of the water load on the projectile's head kinetic energy is shown in Figures 5.8 and 5.11. These charts show that this effect is pronouncedly extremal. Although it is quite obvious that the increase of powder charge increases kinetic energy, the effect of nozzle length is more complicated. At a higher charge the effect of the water load is stronger than at the lower charge. The length of the nozzle also affects kinetic energy of the projectile head. Figure 5.11 shows that the extremum of the kinetic energy shifts to the higher loads as the length of the nozzle

increases. At the same time the absolute value of the maximum does not depend on the nozzle length.

The amount of water loaded in the cannon also has a significant effect on the firing. As it is seen from Figure 5.7, the different water loads provide different outflow profiles: the less the water load the greater the maximum outflow speed and the shorter the projectile head, which is the effective length of the projectile. Figure 5.8 depicts kinetic energy of the projectile head as a function of water load for different powder charges.

The nozzle exit diameter also significantly affects the kinetic energy of the projectile head. The smaller the diameter the shorter the projectile head and the higher the maximum water velocity. The kinetic energy integral as a function of the nozzle exit diameter at different water loads is depicted in Figure 5.10. The steep rises in the graphs are due to the early cut off of the projectile head defined by the coefficient of 0.85. However, in all cases the maximum of the kinetic energy of the projectile head is not affected. This is clearly seen in the region of 15-18mm of the collimator diameter.

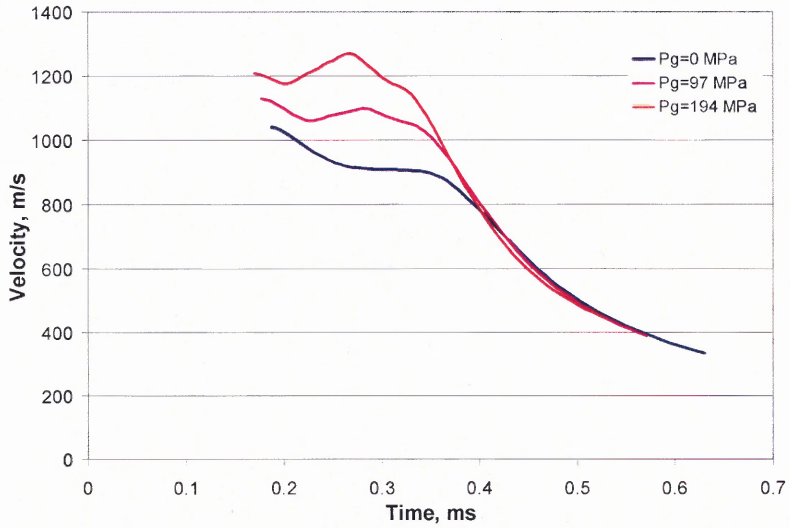

Figure 5.9 Outflow velocity vs. time at different gas pressures acting on the slug during its flow in the nozzle.

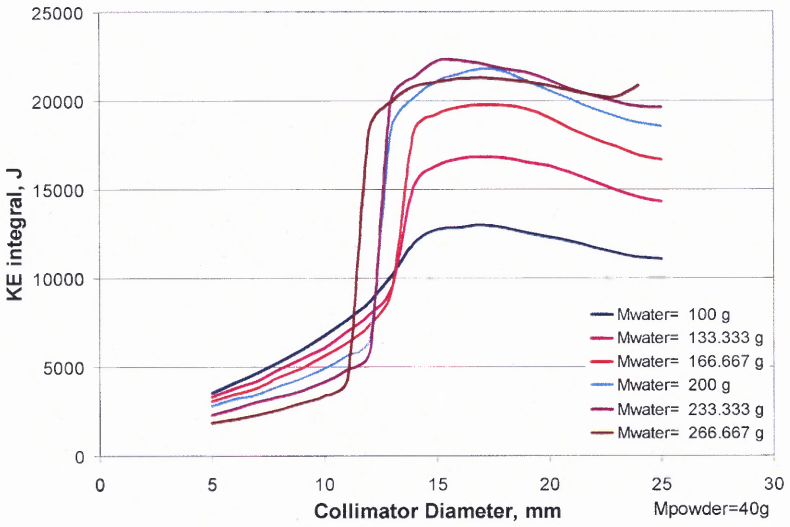

Figure 5.10 Integral Effective kinetic energy vs. nozzle diameter at different water loads.

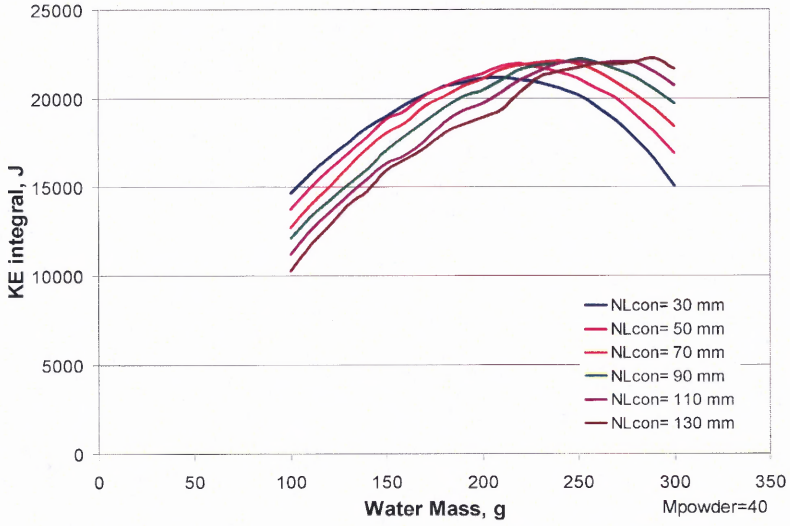

Figure 5.11 Kinetic energy integrals vs. water loads at different nozzle lengths.

5.4 Water Cannon Design Optimization

5.4.1 Problem Statement

Construction of any device involves a series of decisions. These include the principle of operation, design concept and finally selection of parameters defining specific device. Each of these steps can be an independent research effort involving large teams or even

institutions. The selection of the optimal design parameters is considered in this chapter conformably to the water cannon.

The selection of the optimal parameters involves finding parameters values at which some function, termed an optimization criterion, is maximized or minimized. If there are restrictions imposed on the domain of these values, a problem is called constrained optimization and constitutes a section of the mathematical discipline of optimization.

In the general case the problem is to find

$$\min_{x \in \Re^n} f(x) \tag{5.17}$$

subject to

$$\begin{aligned} &G_i(x) = 0 \qquad i = 1,...,m_e \\ &G_i(x) \le 0 \qquad i = m_e + 1,...,m \\ &x_l \le x \le x_u \end{aligned} \tag{5.18}$$

Here x is a vector in $\Re^n$ defining n design parameters. $f(x)$ is the objective function ($f(x)$: $\Re^n \rightarrow \Re$), and $G_i(x)$ are the constraint functions.

A number of parameters define the water cannon design. Only the internal geometry of the simplest water cannon is defined by six variables. Twelve parameters describe the powder charge. Water projectile formation and its outflow are complex processes that cannot be described analytically with sufficient accuracy. Numerical modeling using Godunov's method is used for numerical process approximation. Understanding of these processes and the influence of some of the parameters is achieved by numerous calculations and physical reasoning. However due to non-linearity and large number, it is not possible to comprehend how different parameter combinations can influence the outflow parameters. Thus, it is essential for optimal water cannon design to

develop automatic search procedures for the design parameters optimizing water cannon operation.

Unconstrained optimization Problem (5.17) considered without any of the constraints (5.18) is called a problem of unconstrained optimization. Algorithms for solving this problem serve as a basis for solving more general problems of constrained optimization. The general idea of these algorithms is the construction of monotonic sequence $f(x^j)$: $\forall j \in \mathbb{N}\, f(x^j) < f(x^{j-1})$ starting from some initial approximation x^0.

Coordinate-wise descent methods search for the local minimum by constructing x^j in a form $x^j = x^j + se_k$, where e_k is the k-th basis vector in $\mathbb{R}^n$. The *step of descent* s is defined by

$$\min_{s \in \mathbb{R}} f(x^j + se_k) \tag{5.19}$$

Solution of (5.19) is a separate problem called *linear search.* The index k cyclically changes from 1 to n at each step j.

The method of steepest descent appears to be more effective then coordinate-wise descent and differs from it in selection of the direction from x^j to x^{j+1}. A gradient $\nabla f(x)$ is calculated at each step and the problem (5.19) evolves to

$$\min_{s \in \mathbb{R}} f(x^j + s\nabla f(x)) \tag{5.20}$$

In *the method of random descent* the direction from x^j to x^{j+1} is selected randomly at each step. Its main drawback is that a random descent direction **a** leads further from $\nabla f(x)$ at higher dimensions of the optimization domain.

While the convergence of the described methods can be proved under certain conditions, their effectiveness is still an actual issue. Even smooth functions can fail to be

efficiently minimized by the described approaches. One of these functions is the Rosenbrock's function

$$f(x) = 100(x_2 - x_2^2)^2 + (1 - x_1)^2 \tag{5.21}$$

Its main peculiarity is the long narrow valley leading to a minimum at x=(1,1). In Figure 5.11 taken from the MATLAB User Manual, the process of minimizing this function using the descent algorithm is shown. The optimization stopped after 1000 calculations, still far from the point where the function assumes a minimum. Rosenbrock's function is an example of a function that has an ill-conditioned Hessian matrix $H_{ij} = \dfrac{\partial^2 f(x)}{\partial x_i \partial x_j}$. For these matrices, steepest descent quickly leads to a valley, after which it starts zigzagging as it slowly progresses to the point of the minimum.

Newton-type methods address this issue. These methods evaluate the curvature of the function at each iteration and resolve the following quadratic-form problem

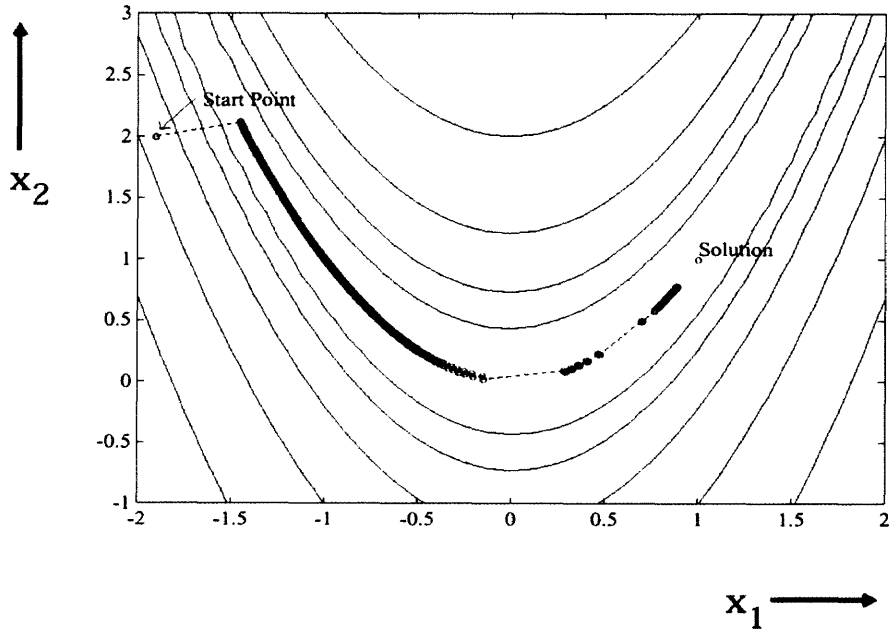

Figure 5.12 Steepest Descent Method on Rosenbrock's Function (Eq. 5.21). Source: from MATLAB User Manual.

$$\min_{x\in\mathbb{R}^n} \frac{1}{2}x^T Hx + c^T x + b, \tag{5.22}$$

where H is the Hessian matrix, and c and b are constant vectors. The solution of the problem (5.20) occurs at a point x^* : $\nabla f(x^*)=0$. Thus $x^*=H^{-1}c$.

However it is very computationally expensive to calculate H at each time step especially for higher dimensional problem.

Quasi-Newton methods avoid this by updating the Hessian using single evaluations of the function at each iteration. The approximation method BFGS developed by Broyden, Fletcher, Goldfarb and Shanno (Broyden, 1970, Fletcher, 1970, Goldfarb, 1970, Shanno, 1970) is considered to be the most effective. In this case the starting point of the Hessian cannot be positively defined, which will lead to infinity when solving 1.4. Thus H initially can be taken as an arbitrarily positively defined matrix, or alternatively the method of steepest descent can be used for first few iteration until a valley is reached.

The BFGS Quasi-Newton method is used in these Matlab Optimization Toolbox functions:

fminunc – Unconstrained nonlinear minimization

fmincon – Constrained nonlinear minimization

The Nelder-Mead Simplex Search Method realized in the *fminsearch* Matlab function is a direct search method and does not require numerical or analytical gradients as Quasi-Newton methods do. Thus although not as effective in general as the BFGS Quasi-Newton Method, this direct search method is more robust and often can handle discontinuities.

The idea behind the method is construction of a simplest nondegenerate figure in n-dimensional space. The figure would consist of n+1 vertices and have non-zero volume

in n-dimensional space. For n=2 the simplex is a triangle, for n=3 it is a tetrahedron. After construction of the initial-guess simplex, the figure is transformed in the search for a minimum. The transformation algorithm is such that the simplex makes its own way down to a local minimum. Due to its robustness and availability in the Matlab Math Library the *fminsearch* function was used in the nozzle profile optimization problem.

However the Nelder-Mead Simplex Method (Nelder and Mead, 1965) may not converge to the local minimum if it is located on a discontinuity, which was the case for the nozzle profile optimization problem.

The other unresolved issue is that the tested and employed algorithms are local minimum search methods. Generally, in engineering a global minimum search problem is to be solved in order to find the optimal design parameters on the permissible domain. *Systematic search* and *random search* methods can be employed in solving this global optimization problem.

The general idea behind the simplest systematic search is uniform meshing of the optimized function domain with subsequent selection of a function maximum over the mesh nodes. Then the new meshing is done on a smaller region around the maximum with a smaller mesh size. After the node of maximum function value is found, the process repeats until the desired accuracy is reached. The main drawback of the method is exponential growth of the required function evaluations with increase of the domain dimension n.

A random search method is more realistic and more frequently used. Global minimum search here is accomplished by evaluation of the objective function at the points initially uniformly randomly scattered over the optimization domain. The

distribution of evaluation points subsequently becomes more and more concentrated around the current function maximum. This method is mathematically proved to converge to the global minimum over compact space in n-space $\mathbb{R}^n$. The main challenge in realization of this algorithm is uniform random number generation. One type of modifications of this method is the *Genetic Algorithm; it* successfully used in many areas of science and engineering.

5.4.2 Nozzle Geometry Optimization

Matlab optimization toolbox algorithms were incorporated into the program for simulating water cannon operation. The implemented procedures search for unconditional local maximum in the unbounded multivariable space. The following notations were used in these calculations

The developed procedure was used for the optimization of the nozzle shape. The nozzle geometry was approximated by two intersecting cones.

The length of the nozzle and its inlet and outlet diameters were constant and equal to

$$L_{nzl}=0.07m,\ R_{inlet}=0.016m,\ R_{outlet}=r_{col}=0.0075m \tag{5.23}$$

Thus a region in two-dimensional space was formed, where x represented the length of the first cone, and y –the radius of the cones intersection. This region in x-y space was determined by the constraints of the position of the cones connection. It should be more than zero and less than the total length of the nozzle. The constraints were also imposed on the radius of the intersection that should vary between radii of inlet and outlet cross sections. Finally, the convergence angles should be not exceeding 45°. Thus

$$x = L_{con1} \in [0,\ 0.07] \tag{5.24}$$

$$y = R_{con1} \in [0.0075,\ 0.016] \tag{5.25}$$

$$x + y - 0.016 \geq 0 \tag{5.26}$$

$$x + y - 0.0075 - 0.07 \leq 0 \tag{5.27}$$

The barrel length was adjusted so that the internal volume of the cannon was constant at variable nozzle shape. This constrain is imposed to control the work of the combustion products which depend on the available volume.

The integral of the effective projectile impulse was used as the optimization criterion:

$$I = \pi r_{col}^2 \int_0^{stop} \rho_o v^2 dt \tag{5.27}$$

where t_{stop} is defined by condition $v \geq 0.85\ v_{max}$, i.e. only the relatively fast fraction of the projectile was taken into account, because only this part determines the obstacles destruction. The function calculating the criteria was set to zero when the arguments were out of the allowed region.

The results of the optimization are presented in Figure 5.13.

A consecutive search was run afterwards to check the optimization results and visualize the objective function for the design of a new nozzle. (Figure 5.14)

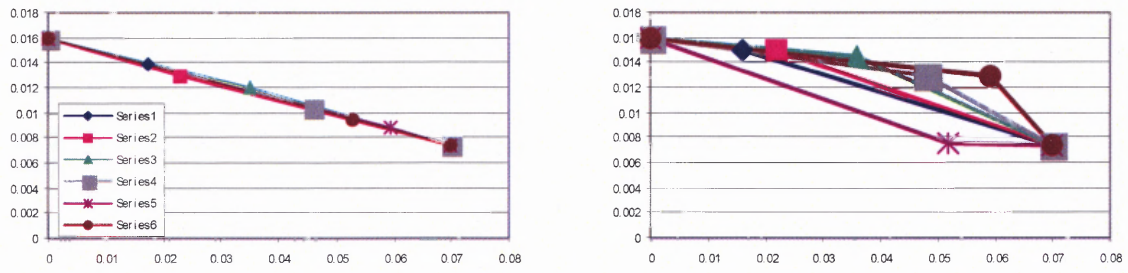

a b

Figure 5.13 Initial a) and optimized b) nozzle profiles.

As it is shown in Figure 5.14, the maximum of the selected criterion is located in the region of the maximal convex curvature and the maximal length of the first cone. Objective function varies 16% on the selected region, while the maximal velocity shows only 3% variation. This suggests that the projectile has a very different rate of decrease of the outflow velocity at different nozzle configurations. Thus, the concave nozzle has a lower projectile quality due to faster decrease of the outflow velocity and subsequently its faster disintegration. The chart of the integral of the effective kinetic energy has similar shape because only the mass multiplier significantly varies and the velocity multiplier is about the same.

The developed optimization algorithm can be used for estimation of the water cannon parameters. However in the course of the search of the global extremum several starting points should be used.

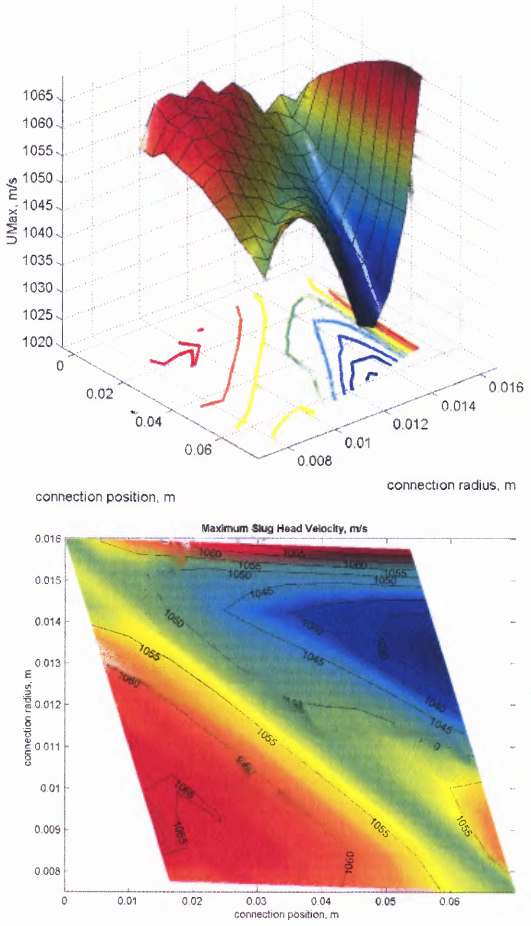

Figure 5.14 Maximum outflow velocity of a slug at different nozzle configurations.

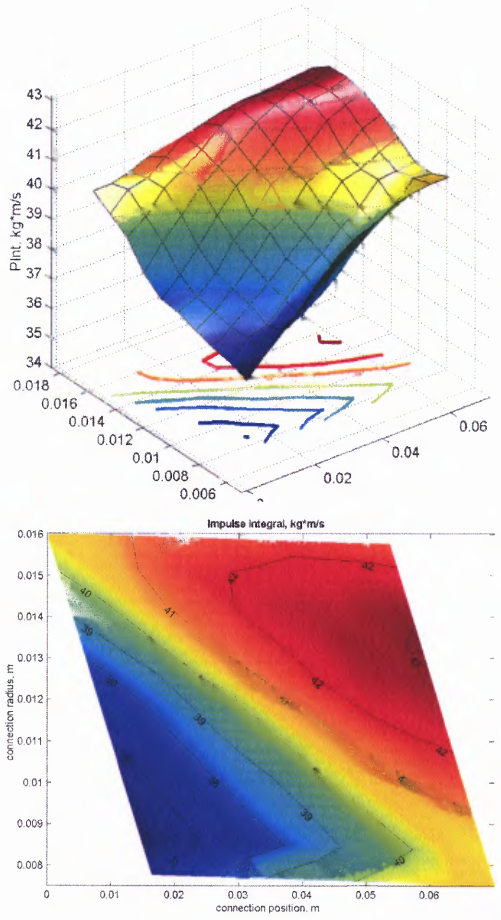

Figure 5.15 Effective momentum integral of a slug at different nozzle configurations.

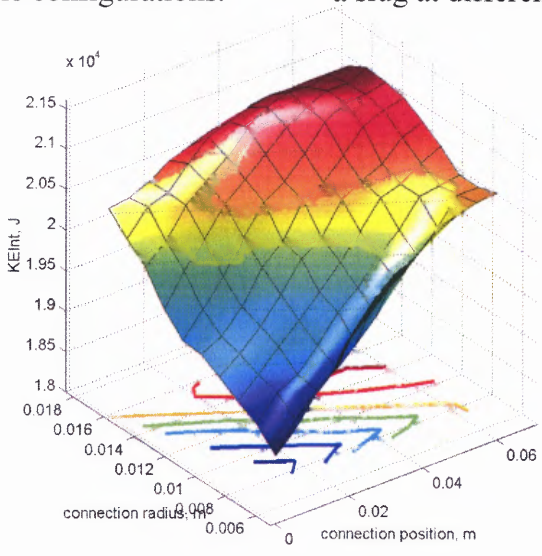

Figure 5.16 Effective kinetic energy integral of a slug at different nozzle configurations.

5.5 Concluding Remarks

The developed numerical model provides complete information on the produced water projectiles. Rather difficult or impossible to acquire experimentally, this information provides new means for experimental study of projectile-target interaction. The results of the projectile impact now can be correlated directly with projectile's velocity distribution, its various integral parameters and their combinations, rather than with gunpowder and water load mass. This empirical model can provide a cannon optimality criterion expressed in terms of projectile parameters rather then in terms of parameters describing the desired target modification.

With this criterion at hand a parametric optimization of the water cannon operation targeted for a specific operation and a specific material becomes feasible. The presented nozzle profile optimization can be extended on the other parameters, describing water cannon geometry, powder charge and water load. Naturally, different target types, materials and operation types would have different optimal values of a water cannons and its charge.

CHAPTER 6

INCOMPRESSIBLE MODEL OF WATER CANNON OPERATION

6.1 Definition of the Model

In the description of internal ballistics of the powder hydro cannon fluid is assumed ideal and incompressible, nozzle profile is smooth, radial flow, heat transfer and atmosphere pressure are insignificant. Quasi-stationary powder combustion occurs on surface in parallel layers by geometric law; the combustion rate depends only on the pressure of powder gases (Petrenko et al., 2002), parameters of powder gases are bonded by a simplified Van der Waals equation. Initiation of the powder ignition is assumed to be a process beginning. Point of origin is located at the nozzle entrance.

In this problem the fluid flow is described by the equations

$$\frac{\partial uF}{\partial x} = 0, \quad \frac{\partial u}{\partial t} + \frac{\partial}{\partial x}\left(\frac{u^2}{2} + \frac{p}{\rho}\right) = 0 \tag{6.1}$$

at initial and boundary conditions

$$u(0,x) = 0, \quad p(0,x) = 0, \quad x_{g0} \le x \le x_{f0}; \tag{6.2}$$

$$p(t,x_f) = 0, \quad p(t,x_f) = 0, \quad p(t,x_g) = p_g, \quad u(t,x_g) = u_g;$$

$$p(t,x_k) = 0, \tag{6.3}$$

Boundary condition $p(t,x_k) = 0$ at the end of collimator is applied at the end of collimator when water flows out.

Gunpowder combustion is described by the following system of the ordinary differential equations with initial conditions (Atanov et al., 1996, Atanov et al., 1977, Petrenko et al., 2004)

$$\frac{dz}{dt} = \frac{u_1}{h_1} p_g; \quad Q_g = m_{p0}\sigma(z)\frac{dz}{dt}$$

$$\frac{dV_g}{dt} = u_g F + \left(\frac{1}{\rho_p} - \alpha\right) Q_g; \quad \frac{dx_g}{dt} = u_g \ ; \tag{6.4}$$

$$\frac{dp_g}{dt} = \frac{1}{V_g}\left[(k-1)q Q_g - p_g\left(k u_g F + \left(\frac{1}{\rho_p} - \alpha\right) Q_g\right)\right];$$

$$z = 0, \ V_g = V_{g0}, \ p_g = p_{g0}, \ x_g = x_{g0}.$$

For an incompressible fluid the partial differential equations (6.1) can be reduced to a system of the ordinary differential equations. From mass conservation equation in the system (6.1) it follows, that velocity of any point in the fluid is related to the velocity of the gas-liquid interface by the equation

$$u(t,x) = u_g(t)\frac{F_g(t)}{F(x)}, \tag{6.5}$$

were subscript "g" designates parameters at the gas-liquid interface. Substituting (6.5) into momentum equation of the system (6.1) and, taking into account that u_g and F_g depend only on t, and F – on x, the following equation is obtained

$$\dot{u}_g \frac{F_g}{F} + \frac{u_g^2}{F} F'(x_g) + \frac{\partial}{\partial x}\left(\frac{u_g^2 F_g^2}{2F^2} + \frac{p}{\rho}\right) = 0, \tag{6.6}$$

where $\dot{u}_g = du_g/dt$, $F'(x_g) = dF/dx$ at $x = x_g$. Component $\frac{u_g^2}{F} F'(x_g)$ appears only for movement of rear interface in nozzle ($x_g > 0$), where the cross section changes along the axis as $F_g = F(x_g)$. In this case in any cross section x velocity will be changing with time even if acceleration of rear interface will be zero ($\dot{u}_g = 0$), due to changing F_g.

Integration of liquid movement equation (6.6) from x to x_f taking into account boundary condition (6.2) $p(t, x_f) = 0$ on the free surface, yields:

$$\left[\dot{u}_g F_g + u_g^2 F'(x_g)\right]\int_x^{x_f} \frac{d\xi}{F(\xi)} + \frac{u_g^2 F_g^2}{2}\left(\frac{1}{F_f^2} - \frac{1}{F^2(x)}\right) - \frac{p(x)}{\rho} = 0.$$

From the equation above it follows that the pressure distribution and liquid movement equation have the form

$$p(x) = \rho\left[\left[\dot{u}_g F_g + u_g^2 F'(x_g)\right]\int_x^{x_f} \frac{d\xi}{F(\xi)} + \frac{u_g^2 F_g^2}{2}\left(\frac{1}{F_f^2} - \frac{1}{F^2(x)}\right)\right], \tag{6.7}$$

$$\dot{u}_g = \frac{1}{F_g}\left\{\left[\frac{p_g}{\rho} - \frac{u_g^2}{2}\left(\frac{F_g^2}{F_k^2} - 1\right)\right]\left(\int_{x_g}^{x_f} \frac{d\xi}{F(\xi)}\right)^{-1} - u_g^2 F'(x_g)\right\}. \tag{6.8}$$

The boundary condition at the exit of the collimator are determined by the equation (6.3). The boundary condition determined by equations (6.2) and (6.3) are essentially the same, however in (6.3) the coordinate x_k is taken as free surface coordinate.

Equations of fluid flow (6.7) and (6.8) contain unknown time depending variables such as powder gases pressure p_g, coordinate x_g and velocity u_g of liquid gas interface, coordinate x_f of free surface and area $F_f = F(x_f)$. Coordinates x_f and x_g are related via equation of mass conservation, which for the inflow stage has form

$$\int_{x_g}^{x_f} F(x)dx = F_c L. \tag{6.9}$$

If nozzle profile is set, then from (6.9) an algebraic equation is obtained after integration, which relates x_f and x_g. However, when solving the fluid governing

equations numerically it is more convenient to use differential not algebraic relation between coordinates

$$\dot{x}_f = u_g \frac{F_g}{F_f}. \tag{6.10}$$

Thus, the internal ballistics of the powder hydro cannon for an ideal incompressible fluid is described by the following system of ordinary differential equations with initial conditions

$$\frac{du_g}{dt} = \frac{1}{F_g}\left\{\left[\frac{p_g}{\rho} - \frac{u_g^2}{2}\left(\frac{F_g^2}{F_k^2} - 1\right)\right]\left(\int_{x_g}^{x_f} \frac{d\xi}{F(\xi)}\right)^{-1} - u_g^2 F'(x_g)\right\}$$

$$\frac{dx_g}{dt} = u_g, \quad \frac{dx_f}{dt} = u_g \frac{F_g}{F_f}$$

$$\frac{dz}{dt} = \frac{u_1}{h_1} p_g, \quad \frac{dV_g}{dt} = u_g F + \alpha_1 Q_g, \tag{6.11}$$

$$\frac{dp_g}{dt} = \frac{1}{V_g}\left[(k-1) q Q_g - p_g\left(k u_g F + \alpha_1 Q_g\right)\right];$$

$$z = 0,\ V_g = V_{g0},\ p_g = p_{g0},\ x_g = x_{g0},\ u_g = 0,\ x_f = x_g + L.$$

Here $Q_g = m_{p0}\sigma(z)\,dz/dt$, $\alpha_1 = 1/\rho_p - \alpha$.

Considering for example a hydro cannon with a conic nozzle, which cross section radius changes according to a law (Atanov et al., 1977): $R = kx + b$, where $k = (R_s - R_c)/L_s$ and $b = R_c$, where R_c, R_s and L_s – radii of nozzle entrance and exit and nozzle length, x_s – coordinate of nozzle end.. Then nozzle cross section area changes according to the law

$$F = \begin{cases} F_c, & x \le 0, \\ \pi(kx+b)^2, & 0 \le x \le x_s, \\ F_s, & x_s \le x \le x_k. \end{cases} \qquad (6.12)$$

Integration of (6.9) yields, for example, for $0 \le x_f \le x_s$

$$\int_{x_g}^{x_f} F(x)dx = -F_c x_g + \frac{\pi}{3k}\left[(kx_f + b)^3 - b^3\right] = F_c L .$$

Then a relation between coordinates x_f и x_g at all stages of the flow development

$$x_f = \begin{cases} x_g + L, & x_g \le x_{gs}, \\ \frac{1}{k}\left[\left(\frac{3kF_c}{\pi}(L + x_g) + b^3\right)^{\frac{1}{3}} - b\right], & x_{gs} \le x_g \le x_{gk}, \\ x_s + \frac{1}{F_s}\left[F_c(L + x_g) - \left(\frac{\pi}{3k}(kL_s + b)^3 - b^3\right)\right], & x_{gk} \le x_g \le 0. \end{cases} \qquad (6.13)$$

Here $x_{gs} = V_s / F_c - L$ – rear interface coordinate at the moment when water completely fills the nozzle, V_s – nozzle volume, $x_{gk} = x_{gs} + V_k$ – coordinate of rear surface at the moment when water fully fills collimator. V_k – collimator volume. During the fluid exit $x_f = x_k = const$ and coordinate x_f does not depend on x_g.

Thus dynamics of hydro cannon for incompressible fluid is governed by the system of the ordinary differential and algebraic equations (6.4), (6.7) and (6.8) with corresponding initial conditions. This problem can be solved numerically, for example using Runge-Kutta method or more simple Euler method.

6.2 Estimation of the Fluid Compressibility Effect

Estimation of fluid compressibility effect on flow parameters can be done as following. The sonic speed of water can be defined as $a = \sqrt{\left(\frac{\partial p}{\partial \rho}\right)_S} = \sqrt{\frac{n(p+B)}{\rho}}$. At the atmospheric pressure this speed is equal to $a_0 \approx 1500$ m/s. It is expected that with increase of the sonic speed, that is decrease of the fluid compressibility, solution of the fluid flow problem converges to the solution for the incompressible fluid flow. Formally this can be done by increasing adiabatic coefficient n in the state equation in the following way: $a_0' = a_0\sqrt{n'/n}$. For example for $n' = 400\ n$ sonic speed is $a_0' = 20\ a_0 = 30$ км/с. If the increase of the sonic speed changes computational results insignificantly, then the fluid compressibility can be disregarded. Otherwise fluid compressibility should be taken into account. The closed form solution available for the incompressible fluid enables us to estimate the accuracy of the computational procedure used for the compressible fluid. If at increase of the sonic speed the solution for the compressible fluid converges to a known solution for incompressible fluid, then the computational procedure is accurate.

The following reasoning could be suggested to corroborate the above considerations. Let us write the continuity of momentum equations of an ideal compressible fluid in the form

$$\frac{d\rho}{dt} + \rho\nabla\vec{u} = 0, \quad \frac{d\vec{u}}{dt} + \frac{1}{\rho}\nabla p = 0. \tag{6.14}$$

Converting equations by exclusion of derivative of ρ over time, obtain

$$\frac{1}{a^2}\frac{dp}{dt} + \rho\nabla\vec{u} = 0, \quad \frac{d\vec{u}}{dt} + \frac{1}{\rho}\nabla p = 0. \tag{6.15}$$

Assume that the velocity and pressure in hydro cannon increase to values u and p over time t on distance L. Then the items in the above equations can be estimated as follows

$$\frac{1}{a^2}\frac{dp}{dt} \sim \frac{1}{a^2}\frac{p}{t},\ \rho\nabla\vec{u} \sim \rho\frac{u}{L},\ \frac{d\vec{u}}{dt} \sim \frac{u}{t},\ \frac{1}{\rho}\nabla p \sim \frac{p}{\rho L}. \tag{6.16}$$

Comparison of the order of items in the momentum equation yields

$$\frac{p}{\rho L} = \frac{u}{t}. \tag{6.17}$$

As the velocity changes over time t on distance L, then $u = L/t$ and thus $p = \rho u^2$, which conform to the Bernoulli equation by the order of magnitude of parameters. Comparing items' order of magnitude in the equation of mass conservation we obtain

$$\frac{1}{a^2}\frac{dp}{dt} : \rho\nabla\vec{u} \sim \frac{1}{a^2}\frac{pL}{t\rho u} = \frac{L^2}{a^2t^2} = \frac{u^2}{a^2} = M^2. \tag{6.18}$$

From the equation above follows that the first item in at $a >> u$ can be disregarded. Then the equations of motion for low-compressible fluid take the form of

$$\nabla\vec{u} = 0,\ \frac{d\vec{u}}{dt} + \frac{1}{\rho}\nabla p = 0. \tag{6.19}$$

The above equation is a standard form of the equation of the incompressible flow. Thus the following three techniques are available for the flow analysis. These techniques include computational solutions of the equations, describing compressible fluid (water). Another solution describes the water flow at condition of the fluid incompressibility. Finally, the solution is obtained for a compressible fluid at a large n, which is termed low compressibility solution.

6.3 Numerical Study Of Water Cannon Operation

The developed numerical technique was used to examine variation of the water velocity at the exit of the hydro cannon as well as the effect of the design and operational conditions on this velocity. The developed models for incompressible, low compressible and compressible fluids were used for process analysis. It is obvious that while the modeling of the compressible flow brings about the most accurate process evaluation, the use of the incompressible model due to its simplicity makes the process analysis much more practical. Moreover, the closed form solution attainable at the application of the incompressible model enables us to use a rigorous optimization technique for the cannon design. The assumption of the process incompressibility is valid only at the fluid velocity below sonic. Of course, the error resulted from the assumption of the process incompressibility limits such applications, especially at supersonic fluid velocity and, thus, should be evaluated. The performed computations were used for such an evaluation, which shows the conditions of the applications of the model in question. The comparison of the computational results obtained at different assumptions (incompressible, low-compressible and compressible) indicates the accuracy of the computations. Indeed, if the procedure is sufficiently accurate, the difference of the water velocities determined by the use of two different models involving low or no compressibility should be insignificant. The performed computations also show the effect of various process variables on the exit water velocity. The most important information which can be obtained as the result of the computations is estimation of the maximal potentially available water velocity as well as the time interval when this velocity is generated.

The charts depicting variation of the exit water velocity and the pressure of combustion products during the water expulsion by the powder combustion products process were constructed for various process conditions and the form of the constructed charts were used for process evaluations. The charts in Figure 6.1 shows process results at the operational conditions which were maintained in the course of performed experiments. The principal feature of the chart is similarity of the results of computation for incompressible and low-compressible fluids. Although the numerical techniques are completely different, the computed patterns of the velocity change at both assumptions are almost identical. The maximal velocities in both cases (1,254 m/s for incompressible and 1,450 m/s for low-compressible) attained at the process beginning differ by 196 m/s (almost 14%). However this difference drops as speed of the water drops. At the speed of 1,500 m/s (sound speed in water at room conditions) two patterns became identical, as it is predicted by the analysis of the balance equations. The computed initial value of the velocity of a compressible fluid is 1,050 m/s which is below velocity of the incompressible liquid by 204 m/s. (about 16%). The pattern of the change of the velocity

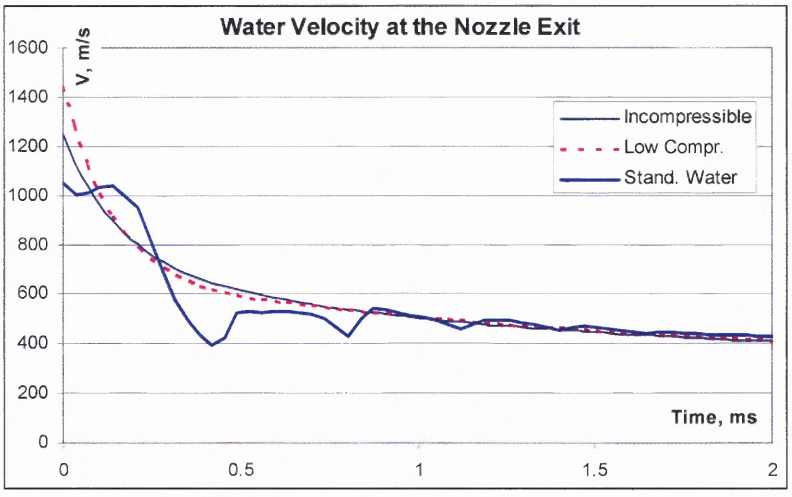

Figure 6.1 Variation of water velocity at the exit of a hydro cannon nozzle for different fluid models.

of compressible liquid is also different. In the beginning of the exit the velocity of this fluid is almost constant (1,000 – 1,050 m/s). This plateau is due to the release of the internal energy accumulated in the compressible medium. After release of this energy and its converging in the kinetic energy of the stream, the behavior of the compressible and incompressible fluid becomes very much similar.

Process results at various potentially possible conditions were computed in order to determine process peculiarities. Charts in Figure 6.2 show the effect of the barrel length on the exit velocity. In this case the length of the barrel was about 8 times more than that used in the experimental device. Due to increase of the momentum exchange between the combustion products and water the water velocity at the beginning of the process reached 1,870 m/s. However the computed pattern of velocity variation does not changed significantly.

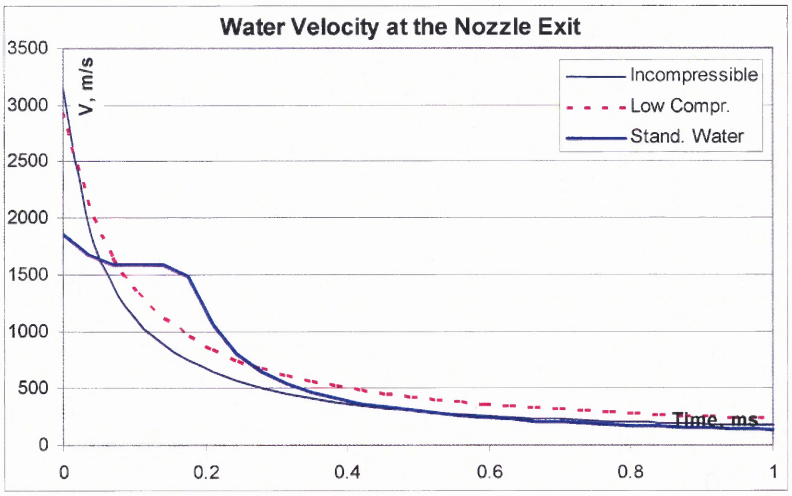

Figure 6.2 Outflow velocity for cannon of 3m barrel length.

Significant increase of the water velocity was achieved at the increase of the amount of powder and reduction of the water load. Chart in Figure 6.3 shows variation of the exit water velocity at the powder mass equal to 700g, the water mass equal to 115g,

and the barrel length equal to 2m. At these conditions the water velocity reached 8,000 m/s, while the maximal velocity of the incompressible fluid was 14,000 m/s. There was no velocity plateau in this case and velocity change of both compressible and incompressible fluids has the form of the hyperbola.

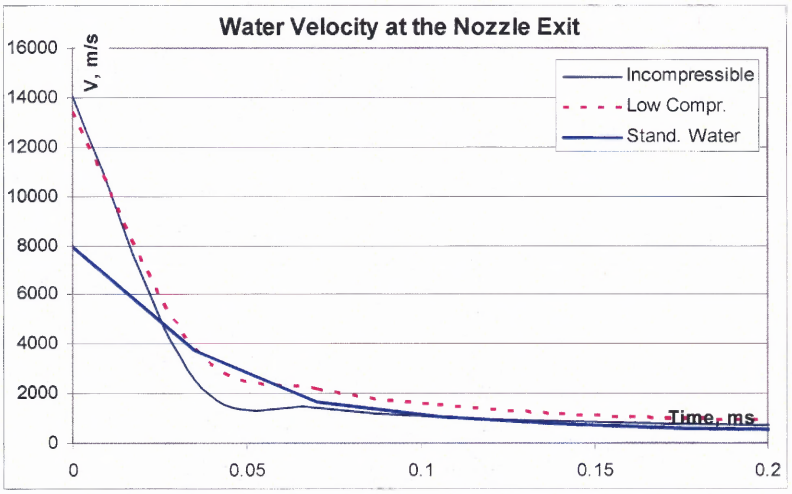

Figure 6.3 Outflow velocity of 115g water load, with 700g powder and 2m barrel.

Increase of the water mass in 4 times changes the velocity pattern dramatically (Figure 6.4). The maximal water velocity drops to 3,000 m/s, however more than 50% of the fluid was expelled at the nearly constant (2500 m/s) velocity.

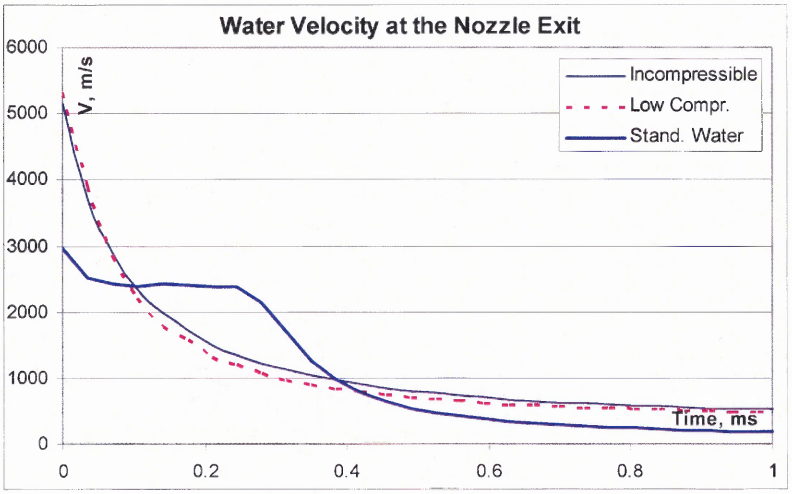

Figure 6.4 Outflow velocity of 460g water load, with 700g powder and 2m barrel.

Dramatic change in the velocity pattern was observed at the increase of the length of the collimator (Figure 6.5). In this case the maximal water velocity was only 1,110 m/s. However if at a short collimator significant velocity was maintained only during 0.1-0.2 millisecond and then drops 3-4 times, at a long collimator the exit velocity drops less then 2 times. This change is due to the velocity redistribution along the water stream during the flow through the collimator. In this case, the patterns of the velocities variation of incompressible and low compressible fluids were substantially different.

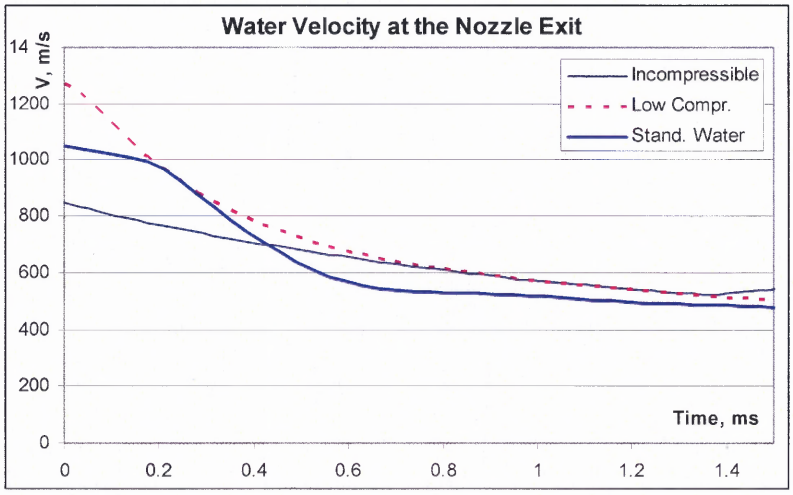

Figure 6.5 Velocity of water outflow from a cannon with long collimator (0.4m)

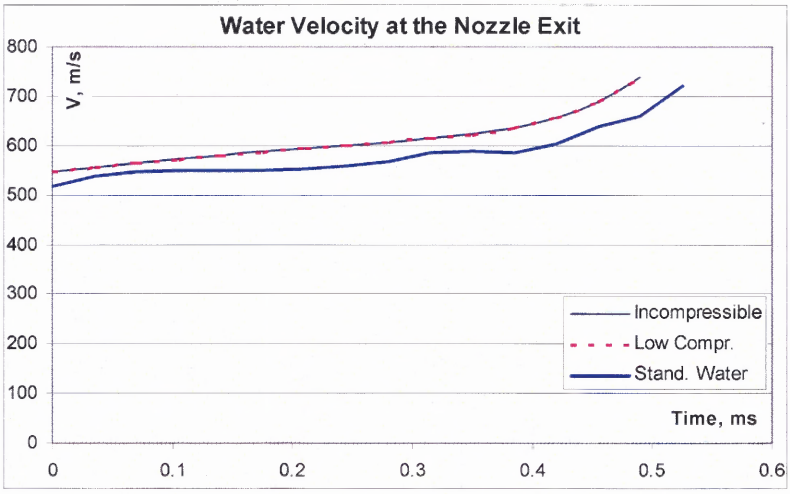

Figure 6.6 Velocity of water outflow from a cannon with nozzle exit 0.94 of barrel dia.

Even more dramatic effect on the fluid velocity pattern has the change of the nozzle diameter. At the exit nozzle diameter equal to 0.94 of the barrel diameter (Figure 6.6) the velocity of the fluid increases, rather than drops in the course of the exit, while the maximal water velocity attained at the end of the process was only 700 m/s. The patterns of the behavior of the compressible and incompressible fluids were practically the same. Reduction of the nozzle diameter (Figure 6.7) brought about the velocity pattern similar to that obtained in previous conditions. The chart Figure 6.7 clearly shows

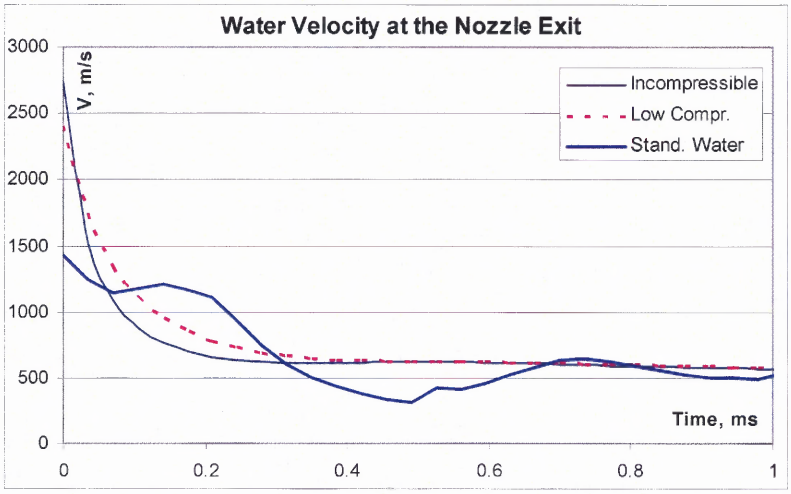

Figure 6.7 Velocity of water outflow from a cannon with nozzle exit 0.34 of barrel dia.

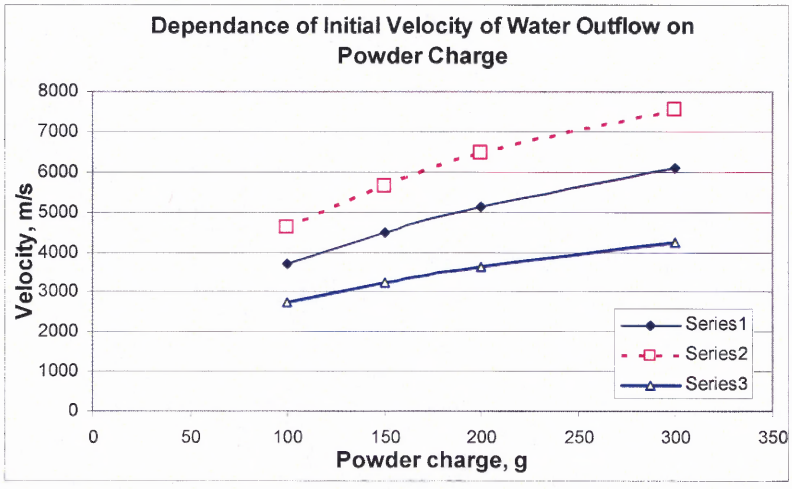

Figure 6.8 Effect of the powder charge mass on initial outflow velocity

presence of the wave processes in the course of the exit of the compressible flow.

The performed computations (totally about 200 cases) enables us to estimate the effect of the various design parameters on the exit velocity. The chart Figure 6.8 shows the effect of the powder mass and the chart Figure 6.9 shows the effect of the nozzle diameter on the exit water velocity. These charts give clear qualitative correlation between process output and process parameters. It should be noted that while velocity magnitude is quite different, the pattern of the constructed relations for the compressible and incompressible fluids are similar. Thus, a simplified numerical procedure developed for the incompressible fluid could be used for process design.

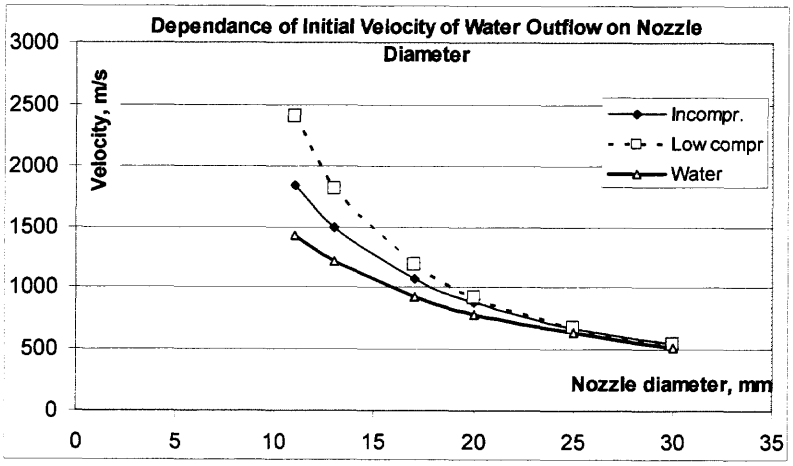

Figure 6.9 Effect of nozzle diameter on initial outflow velocity

6.4 Mechanism of Fluid Acceleration

Explosion-based water acceleration in a hydro cannon is an extremely complicated process, involving multiphase 2D flow of a reacting fluid. It is important from both practical and theoretical considerations to understand the mechanism of momentum transfer from combustion products to the water load. In the barrel of the hydro cannon fluid is accelerated by the expanding combustion products similarly to a

solid. The additional fluid acceleration is attained due to wave superposition in a moving fluid, fluid converging in a nozzle and the unsteady radial flow of the fluid in the nozzle. Comparison of the velocity variation of compressible and incompressible fluids shows that the effect of the wave processes on the fluid acceleration is minimal. The fluid compressibility determines accumulation of the internal energy in the fluid, but has minimal effect on the fluid acceleration.

6.5 Concluding Remarks

The performed computations showed that the fluid compressibility significantly affect flow in the hydro cannon. Calculations for an incompressible fluid yield higher values of pressure and velocity, than those for a compressible one. However, while the numerical values in both cases are different, the process patterns are very much the same. Fluid compressibility in a powder hydro cannon effects the fluid behavior via the undulatory processes, when the duration of these processes is comparable with time of the fluid inflow into the nozzle. Thus estimation of hydro cannon parameters and their optimization can be accomplished using the model of the incompressible fluid, operating with more simple ordinary differential equations rather than much more complicated partial differential equations for compressible fluid. This becomes important for a numerical optimization of water cannon involving many parameters. With more then a dozen parameters describing cannon geometry, liquid and powder parameters, optimum search would require a large number of computations. Employing an incompressible flow model as an initial approximation significantly reduces computational optimization time.

CHAPTER 7

CONCLUSION

The experimental study of water projectiles generated by a water extruder and a water cannon has demonstrated the feasibility of various technologies of material processing with high-speed liquid projectiles. Proof of concept was done for piercing and stamping of metal plates, demolition of concrete, and neutralization of explosive devices.

The experiments have shown that the projectile's size and velocity have a highly non-linear effect on target deformation. In the case of concrete demolition, it was found that below some velocity threshold, the projectiles remove very little amount of material. Thus it is important to produce larger and faster liquid projectiles.

The study of the developed numerical model of projectile formation provided new understanding of the roles played by different cannon parameters and their significance or insignificance. Projectile velocities of several km/s have been shown feasible and the parameters of a cannon and the charge necessary to reach such high velocities has been estimated.

Comparison of compressible and incompressible fluid flow models has shown that fluid compressibility plays a damping role in projectile generation. The reduction of fluid compressibility yields higher head velocities of shorter projectile head. Thus projectile formation in a water cannon is more of inertial than interference of waves nature.

A better understanding of the projectile formation principles and numerical optimization provides the means for developing the emerging material processing technology employing high-speed liquid projectiles.

REFERENCES

1. Conn, A.F. (1998). On Fluid Dynamics of Working Waterjets: Continuous, Pulsed and Cavitations, *Proceedings 5th Pacific Rim International Conference on Waterjet Technology*, Japan, pp. 9-23.

2. Labus, T.J., (1991). Pulsed Fluid Jet Technology, *Proceedings of 1st Asian Conference on Recent Advances in Jetting Technology* (pp. 136-143). Singapore: CI-Premier.

3. Li, Z. Geskin, E.S. (1994). Computer Aided Simulation of Turbulent Flow in Pulsate Jet Nozzle. *14th International Computers in Engineering Conference*, Hawaii.

4. Li, Z., Geskin, E.S. (1994). Numerical Analysis of Waterjet Flow in a Pulsative Jet Nozzle. *7th International Symposium on Transport Phenomena in Manufacturing Processes*, Mexico.

5. Mazurkevich, M. (1984). The Analysis of High Pressure Waterjet Interruption through Ultrasonic Nozzle Vibration, *Proceedings of 7th International Symposium on Jet Cutting Technology, BHRA* (pp. 531-536). Cranfield, Bedford.

6. Vijay, M.M., (1998). Pulsed Jets, Fundamentals and Applications. In A. Momber (Ed.), *Water Jet Applications in Construction Engineering* (pp. 19-41). Rotterdam, Netherlands: Balkema.

7. G.G. Yie, (1978). Performance of a High-Pressure Pulsed Water-Jet Device for Fracturing Concrete Pavement, *Proceedings of 4th International Symposium on Jet Cutting Technology, BHRA Fluid Engineering* (pp. H6-67 – H6-86), Canterbury, England.

8. U.H. Mohaupt, et al., (1978). Design and Dynamic Response of a Pulse-Jet Pavement Breaker, *Proceedings of 4th International Symposium on Jet Cutting Technology, BHRA Fluid Engineering* (pp. D2-17– D2-28). Canterbury, England.

9. Chermensky, G.P., (1976). Breaking Coal and Rocks with Pulsed Water Jets, *Proceedings of 3rd International Symposium on Jet Cutting Technology, BHRA Fluid Engineering* (pp. D4-33 – D4-50), Chicago, USA.

10. Atanov, G.A., (1987). *Hydro-Impulsive Installations for Rock Breakage*, (Russian), Kiev, Ukraine: Vishaia Shcola.

11. Cooley, W.C. (1972). Rock Breakage by Pulsed High Pressure Water Jets, *Proceedings of the 1st International Symposium on Jet Cutting Technology, BHRA* (pp. 101-112). Cranfield, Bedford.

12. Patent No. V 2132, USSR

13. E. A. Antonov, (1961). *Some issues of the theory and practice of water streams*, Ph.D. Thesis, Novosibirsk, Russia.

14. Stanyukovich, K.P., (1955). *Nonsteady Motion of Continuous Media*, (Russian). GITTL, Moscow, Russia.

15. Lavrentjev, M.A., Antonov E.A., Voitcehovsky, B.V., (1961). *Problems of Theory and Practice of Impulsive Water Streams*. IG SO AN USSR, Novosibirsk, Russia.

16. Lavrentjev, M.A., Antonov E.A., Voitcehovsky, B.V., (1960). Theory and Practice of Impulsive Flows, *All-Union Conference on Hydraulic Coal Mining*. Stalinsk, Russia.

17. Chermensky, G.P., (1976). Experimental Investigation of Reliability of Water Cannons, *Proceedings of 3rd International Symposium on Jet Cutting Technology, BHRA Fluid Engineering* (pp. H1-1 – H1-14). Chicago, USA.

18. Edney, B.E., (1976). Experimental Studies of Pulsed Water Jets, *Proceedings of 3rd International Symposium on Jet Cutting Technology, BHRA Fluid Engineering* (pp. B2-11 – B2-26). Chicago, USA.

19. Daniel, I.M., (1976), Experimental Studies of Water Jet Impact on Rock and Rocklike Materials, *Proceedings of 3rd International Symposium on Jet Cutting Technology, BHRA Fluid Engineering* (pp. B3-27 – B3-46). Chicago, USA.

20. A.J. Watson, F.T. Williams and R.G. Brade, (1976). The Relationship Between Impact Pressure and Anatomical Variations in a Water Jet, *Proceedings of 7th International Symposium on Jet Cutting Technology, BHRA Fluid Engineering* (pp. 193-209). Ottawa, Canada.

21. Atanov, G.A. (1977). *Internal Ballistics of Hydrocannon and Impulsive Water Extruder.* Doctor of Science Thesis, Donetsk, Ukraine.

22. E. S. Petrenko, (2002). Disruptors of explosive devices and other explosive objects, *Special Techniques*, 3.

23. United Nations Children's Fund (UNICEF) www.unicef.org

24. International Campaign to Ban Landmines (ICBL) www.icbl.org

25. Orlov, B.V. (1974). *Design of rocket and barrel systems.* Moscow: Mashinostroenie. 382 p.

26. Matlab User Manual, Mathworks Inc.

27. Broyden, C.G. (1970). The Convergence of a Class of Double-rank Minimization Algorithms. *J. Inst. Maths. Applics.*, 6, 76-90.

28. Fletcher, R. (1970) A New Approach to Variable Metric Algorithms. *Computer Journal*, 13, 317-322.

29. Goldfarb, D. (1970). A Family of Variable Metric Updates Derived by Variational Means, *Mathematics of Computing*, 24, pp.23-26.

30. Shanno, D.F. (1970). Conditioning of Quasi-Newton Methods for Function Minimization, *Mathematics of Computing*, 24, 647-656.

31. Nelder, J.A., Mead, R. (1965). A Simplex Method for Function Minimization. *Computer Journal*, 7, 308–313.

32. Atanov, G. A, Gubsky, V. I., Semko, A. N. (1996). The Pressure Rise Factor For Powder Hydro-cannon. *Proceedings of the 13th International Conference on Jetting Technology* (pp. 91-103). Sardinia, Italy: October 29-31.

33. Atanov, G. A., Gubskiy, V.I., Semko, A.N. (1977). Internal ballistics of powder hydrocannon. *Izv. RAN. Mechanics of liquid and gas*, 6, 175–179.

34. Petrenko, O. P. Geskin, E. S., Atanov, G. A., Semko, A. N., Goldenberg, B. (2002). Numerical Modeling of High-Speed Water Slugs, *Proceedings of International Mechanical Engineering Congress and Exhibition (IMECE2002).* November, New Orleans, LA.

35. Petrenko, O. P. Geskin, E. S., Atanov, G. A., Semko, A. N., Goldenberg, B. (2004) Numerical Modeling of High-Speed Water Slugs. *Transaction of the ASME. Journal of Fluids Engineering,* 126(2), 206 – 209.

36. Godunov, S.K., Zabrodin, A.V., Ivanov, M.Y., Kraiko, A.N., Prokopov, G.P. (1976) *Numerical solution of multidimensional problems of gas dynamics*. Moscow: Nauka.